

IMPACT: An Implicit Active-Set Augmented Lagrangian for Fast Contact-Implicit Trajectory Optimization

Jiayun Li^{1,2} Dejian Gong¹ Georgia Chalvatzaki^{1,2,3}

¹PEARL Lab, Dept. of Computer Science, TU Darmstadt, Germany
²Hessian.AI, Darmstadt, Germany, ³Robotics Institute Germany (RIG)

Abstract—Contact-implicit trajectory optimization (CITO) has attracted growing attention as a unified framework for planning and control in contact-rich robotic tasks. Recent approaches have demonstrated promising results in manipulation and locomotion without requiring a prescribed contact-mode schedule. It is well known that the underlying *mathematical programs with complementarity constraints* (MPCCs) remain numerically ill-conditioned, and systematic, scalable solution strategies for CITO remain an active area of research. More efficient and principled solvers that can handle contact constraints are therefore essential to broaden the applicability of CITO. In this work, we develop an augmented-Lagrangian approach to CITO for solving MPCC-based CITO with stationarity guarantees. The method can be interpreted as *identifying the implicit contact-mode branches on the fly during the trajectory optimization (TO) iterations*; we call this approach IMPACT (*IMPlicit contact ACtive-set Trajectory optimization*). We provide an efficient C++ implementation tailored to trajectory-optimization workloads and evaluate it on the open-source CITO and *contact-implicit model predictive control* (CI-MPC) benchmarks. On CITO, IMPACT achieves $2.9 \times - 70 \times$ speedups over strong baselines (geometric mean $13.8 \times$). On CI-MPC, we show improved control quality for contact-rich trajectories on dexterous manipulation tasks in simulation. Finally, we demonstrate the proposed method on real robotic hardware on a T-shaped object pushing task.

I. INTRODUCTION

Optimal motion planning in contact-rich manipulation settings remains one of the major challenges in robotics. The planner must reason not only about continuous dynamics, but also about discrete events in which contacts are established, maintained, and broken to perform tasks such as underactuated manipulation and legged locomotion [1, 2]. This hybrid, nonsmooth structure makes it difficult to cast the problem as a well-defined continuous TO problem. A common workaround is to prescribe the contact mode sequence (contact schedule) a priori; conditioned on this discrete choice, the resulting TO problem can often be formulated as a smooth *nonlinear programming* (NLP) and solved efficiently using existing continuous optimization methods [3, 4]. By contrast, when the contact schedule is not fixed, the problem is typically posed as CITO. While CITO is promising for autonomously inferring contact modes in complex tasks, it is generally more challenging to solve due to nonsmooth contact dynamics and the combinatorics of mode changes [5, 6, 7].

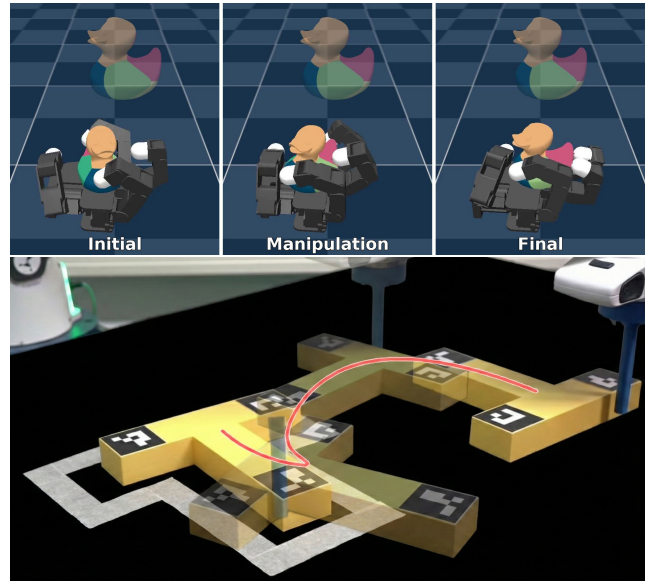


Fig. 1: IMPACT demonstrations in simulation and hardware. **Top:** Allegro Hand reorients a rubber duck in simulation. **Bottom:** a Panda robot pushes a T-shaped block to a target pose in real-robot experiments; the red curve indicates the trajectory of the block’s coordinate origin during the push.

CITO commonly relies on contact models with a complementarity structure to capture the on/off nature of contact and frictional interaction, and the exact form depends on the chosen contact model (e.g., rigid vs. compliant, Coulomb vs. regularized friction) [8]. This yields a fundamentally nonsmooth optimization problem that is naturally cast as MPCCs [9]. At feasible points, complementarity induces degeneracy and violates the regularity assumptions required by standard smooth NLP constraint qualifications (CQs); consequently, standard constraint qualifications such as the *Linear Independence Constraint Qualification* and the *Mangasarian–Fromovitz Constraint Qualification* typically fail, and the associated Lagrange multipliers may become unbounded, rendering the *Karush–Kuhn–Tucker* (KKT) conditions invalid [9, 10]. Consequently, off-the-shelf NLP solvers based on standard KKT/CQ theory are often numerically brittle for MPCCs: large initial complementarity violations make convergence highly initialization-sensitive and unreliable at TO scale [11].

Due to the nonsmooth and degenerate nature of contact-implicit formulations, a variety of practical treatments have been explored to improve numerical robustness. Broadly, existing methods modify the original complementarity structure through smoothing or relaxation, or by introducing (exact) penalty terms to better fit standard solvers and their convergence assumptions [12, 13, 14]. While these treatments often improve numerical behavior, they can degrade control quality and introduce additional heuristic update parameters that strongly affect efficiency. Moreover, as these modifications are tightened to more closely approximate the original complementarity conditions, degeneracy and ill-conditioning can re-emerge, limiting reliability at TO tasks.

In this work, we propose IMPACT (*IMPLICIT* contact *ACTIVE*-set Trajectory optimization), an *implicit complementarity/contact-branch selection* method for solving MPCC-based CITO, with *stationarity guarantee* for feasible accumulation points under standard assumptions from recent augmented Lagrangian (AuLa) theory [15, 16, 17, 18]. Instead of smoothing or relaxing complementarity constraints, IMPACT retains the original nonsmooth contact constraints and handles them through the AuLa subproblems. Across these subproblems, the approximate Lagrange multipliers and penalty strength guide the selection of the active complementarity branch (contact vs. no-contact), enabling an implicit contact-mode discovery without a prescribed homotopy schedule. Fig. 2 conceptually contrasts relaxation, penalty, and IMPACT on a toy complementarity example. Moreover, this AuLa treatment prevents the multiplier blow-up typically seen in vanilla AuLa formulations for MPCCs. As a result, IMPACT provides a principled alternative to penalty-only methods. Combined with our proposed *block coordinate descent* (BCD) solver for the AuLa subproblems, IMPACT achieves substantially faster convergence than strong baselines in our experiments while maintaining competitive performance. On standard benchmarks, this translates to an order-of-magnitude speedup. Our contributions are summarized as follows.

- **Algorithm.** We introduce IMPACT, an efficient CITO method based on an AuLa scheme for MPCCs, and establish its stationarity guarantee.
- **Implementation.** We provide C++ implementations of IMPACT and the evaluation baselines, with an interface designed specifically for CITO/CI-MPC workloads.
- **Validation.** We benchmark IMPACT against representative baselines on open-source suites: (i) a CITO benchmark and (ii) a MuJoCo dexterous-manipulation benchmark for Allegro-Hand CI-MPC. We further demonstrate the method on real robotic hardware in a Push-T manipulation task.

II. RELATED WORK

This section reviews CITO and CI-MPC methods from two perspectives: (a) approaches that *soften* contact logic to obtain smooth gradients for planning/MPC, and (b) approaches that *retain* nonsmooth contact logic and solve more directly.

A. Smooth / Relaxed Contact Models for Planning and MPC

Many CITO/CI-MPC pipelines replace rigid complementarity with *smooth* or *relaxed* surrogates to enable gradient-based optimization, which can improve numerical behavior but may affect gradient accuracy and closed-loop performance. A common approach modifies the *forward contact model* (e.g., compliant or differentiable contact), yielding smoother derivatives at the expense of strict rigid-contact fidelity [6, 2, 19, 13, 12]. Another line keeps *forward simulation* rigid but targets *differentiable optimization* by regularizing the sensitivity/KKT systems used to compute gradients through contact, enabling fast CI-MPC and relaxed-complementarity DDP variants [20, 21, 22]. Beyond local smoothing, global convex relaxations have been explored for CITO, emphasizing geometric reasoning and contact sequencing [23].

In contrast, our method adopts a *nonsmooth* AuLa viewpoint: we update relaxation via safeguarded multiplier/penalty rules and solve nonsmooth subproblems that explicitly enforce complementarity, aiming to preserve mode transitions and implicitly identify the contact mode.

B. Direct Nonsmooth Treatments of Contact Complementarity

A second class handles contact complementarity more *directly*, reflecting the inherent nonsmoothness of contact (make/break; stick/slide). Two common strategies are penalty/continuation methods and operator-splitting schemes.

Early CITO work introduces elastic (slack) variables and penalizes complementarity violations so that contacts can be “discovered” during optimization [5]. Later pipelines improve reliability via continuation strategies or automatic penalty-update rules [24, 11], and related penalty reformulations also appear in *quadratic programs with complementarity constraints* (QPCC) solvers such as LCQPow [25].

Despite their widespread use, penalty/continuation methods can become numerically stiff and brittle under large penalties, and heuristic schedules may slow convergence [11]. These issues motivate safeguarded AuLa schemes for *general* MPCCs; among penalty-based CITO planners, CRISP is closest to our approach [11].

Operator splitting / ADMM exploits CI-MPC structure by alternating trajectory updates with projections onto contact-feasible sets. The C3 family formulates CI-MPC in a consensus ADMM form with simple, parallelizable subproblems, scaling well to many-contact settings such as planar pushing and multi-contact manipulation [26, 27]. Extensions improve robustness via residual learning [28] and sampling guidance [29], while C3+ accelerates planar pushing through more efficient projections [30]. While C3+ is reminiscent of our emphasis on fast inner solves, it targets an ADMM projection setting that differs from IMPACT.

The ADMM-based methods above typically operate on linearized contact/dynamics. They often produce task-space commands, leading to QPCC-style problems and, in many implementations, an additional task-space tracking layer is required for execution [26, 30]. A recent preprint by Ménager et al. [31], released after the initial submission of IMPACT,

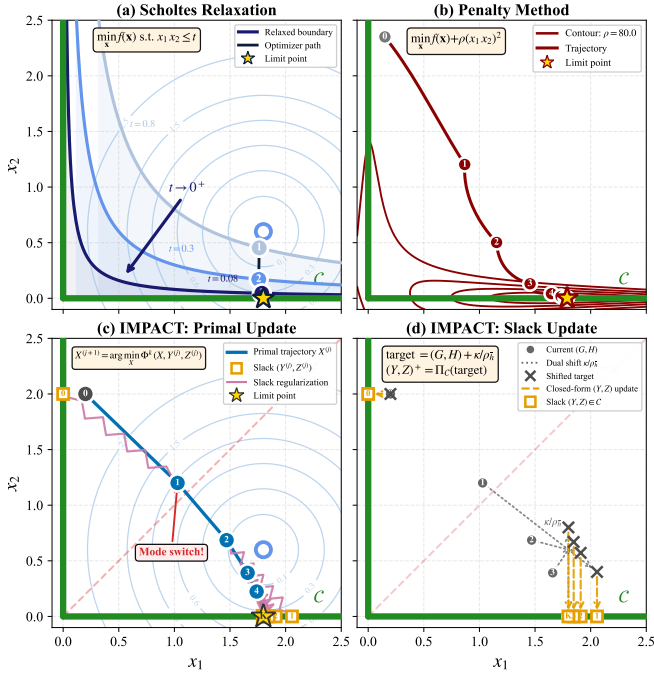


Fig. 2: Comparison of complementarity-handling methods on a 2D toy objective. Top row: Scholtes relaxation and squared-penalty method. Bottom row: IMPACT, split into the primal update and the slack update. Objective contours are shown in blue and the complementarity-feasible set is shown in green. In IMPACT, the slack variables act as anchors that regularize the next primal update, while the slack update is obtained from a dual-shifted target projected onto the complementarity set.

also uses an AuLa and alternating-minimization/BCD scheme for contact-implicit QPCCs in one-step inverse dynamics. In contrast, IMPACT targets temporally coupled TO and CI-MPC settings with general MPCC-based CITO formulations. We use an MPCC-tailored safeguarded AuLa scheme with complementarity-enforcing inner subproblems. This induces an implicit contact-mode selection behavior as slack is driven tight.

III. PROBLEM DEFINITION

In this work, we formulate both CITO and CI-MPC in a unified optimization framework in generalized coordinates, given in problem (1). We use $X = [x_t]_{1:T}$ to denote the trajectory of decision variables (e.g., state, control, and contact forces) over time steps $t = 1, \dots, T$. We use $r(x_t)$, $h(x_t, x_{t+1})$, and $g(x_t)$ to denote the residual function, equality constraints, and inequality constraints, respectively. $h(x_t, x_{t+1})$ consists of the standard equality constraints at time steps t and $t+1$, together with the system dynamics that couple consecutive time steps. The $G(x_t)$ and $H(x_t)$ denote the complementarity functions at time step t . The complementarity condition $0 \leq G(x_t) \perp H(x_t) \geq 0$ encodes a logical exclusivity: component-wise, at least one of $G(x_t)$ or $H(x_t)$ must be zero, so they cannot be simultaneously strictly positive. Algebraically, it is equivalent to $G(x_t) \geq 0$, $H(x_t) \geq 0$, and the element-wise product

constraint $G(x_t) \circ H(x_t) = 0$. Consequently, the problem is inherently nonconvex and nonsmooth. We focus on nonlinear sum-of-squares (SOS) objectives, which capture many task-space motion-planning costs. It is particularly convenient under the AuLa formulation in Section IV, since both the penalty terms and Lagrangian terms can be absorbed into the nonlinear least-squares residual, yielding an efficient Gauss-Newton scheme.

$$\min_X \frac{1}{2} \sum_{t=1}^T r(x_t)^\top r(x_t) \quad (1a)$$

$$\text{s.t. } h(x_t, x_{t+1}) = 0, \quad t \in 1, \dots, T-1, \quad (1b)$$

$$g(x_t) \leq 0, \quad t \in 1, \dots, T, \quad (1c)$$

$$0 \leq G(x_t) \perp H(x_t) \geq 0, \quad t \in 1, \dots, T. \quad (1d)$$

Problem (1) defines a general MPCC, with different discretizations and contact models recovered as special cases. For example, the template accommodates multiple friction models. With a polyhedral approximation of the friction cone, the per-step contact complementarity conditions can be written as a *linear complementarity problem* (LCP). In this case, once the contact Jacobians are fixed at each step (e.g., via a standard linearization or a “frozen Jacobian” approximation), the resulting $G(x_t)$ and $H(x_t)$ are typically affine in the decision variables. If instead friction is enforced using a second-order cone representation, the contact conditions lead to a conic complementarity formulation; this still fits within the same MPCC template, but is generally nonlinear and more challenging to solve.

In particular, our CI-MPC experiments in VI-C adopt the LCP contact model following [13] and use a time-stepping impulse-velocity formulation in the spirit of Anitescu [32]. We directly adopt the KKT system of the primal problem of the Anitescu quadratic program in [13] (Eq. (7)) and incorporate it into the IMPACT formulation:

$$\mathbf{Q}\mathbf{v}_t - (\mathbf{b}(\mathbf{u}_t) + \tilde{\mathbf{J}}_i^\top \beta_t)/h = 0, \quad (2a)$$

$$0 \leq \beta_t \perp \tilde{\mathbf{J}}_i \mathbf{v}_t + \phi_i/h \geq 0. \quad (2b)$$

This system describes the contact dynamics at time step t , where the first line gives the discrete-time dynamics, relating the generalized velocity \mathbf{v}_t through the system mass moment \mathbf{Q} to the actuation/external term $\mathbf{b}(\mathbf{u}_t)$ and the contact-force variable β_t through the contact Jacobian $\tilde{\mathbf{J}}_i$ for the i th detected contact, including the friction-polyhedral approximation and the step size h . The second line imposes complementarity between the contact force β_t and the velocity-level contact residual $\tilde{\mathbf{J}}_i \mathbf{v}_t + \phi_i/h$. Componentwise, a contact-force component can be positive only when the corresponding contact constraint is active, where ϕ_i denotes the normal distance for the i th contact. The generalized velocity \mathbf{v}_t is then related to the generalized coordinate using time integration, possibly involving quaternion integration.

IV. A SAFEGUARDED AULa FOR MPCCS

We next describe the safeguarded AuLa outer loop used in IMPACT. This outer loop updates penalty parameters and

Lagrange multipliers while keeping complementarity enforced explicitly, and provides a stationarity-guaranteed wrapper for our BCD inner solver.

For algorithmic convenience, we rewrite Problem (1) in *vertical form* [10] by introducing auxiliary (slack) variables Y and Z . This moves nonlinearities from the complementarity set into smooth equality constraints: we enforce $G(x_t) = y_t$ and $H(x_t) = z_t$, and impose complementarity directly on the variables via $0 \leq y_t \perp z_t \geq 0$. While this increases the dimension and adds equality constraints, it yields a simple complementarity set that is well-suited to our inner solver design. The resulting vertical form is:

$$\min_{X,Y,Z} \frac{1}{2} \sum_{t=1}^T r(x_t)^\top r(x_t) \quad (3a)$$

$$\text{s.t. } h(x_t, x_{t+1}) = 0, \quad t \in 1, \dots, T-1, \quad (3b)$$

$$g(x_t) \leq 0, \quad t \in 1, \dots, T, \quad (3c)$$

$$G(x_t) = y_t, \quad t \in 1, \dots, T, \quad (3d)$$

$$H(x_t) = z_t, \quad t \in 1, \dots, T, \quad (3e)$$

$$0 \leq y_t \perp z_t \geq 0, \quad t \in 1, \dots, T. \quad (3f)$$

Remark 1. The vertical reformulation is equivalent to the original MPCC: at any feasible point, $(y_t, z_t) = (G(x_t), H(x_t))$, so enforcing $0 \leq y_t \perp z_t \geq 0$ is equivalent to $0 \leq G(x_t) \perp H(x_t) \geq 0$. We adopt this split because AuLa handles the resulting smooth equalities $G(x_t) - y_t = 0$ and $H(x_t) - z_t = 0$ effectively in TO settings [33], while our inner solver exploits the resulting variable-wise complementarity structure via closed-form update (Section V).

We follow a safeguarded AuLa scheme for MPCCs in which complementarity constraints are not absorbed into the augmented Lagrangian function; instead, they are enforced explicitly in each inner solve. Concretely, we handle the smooth equality and inequality constraints via an AuLa treatment, while keeping the complementarity constraints as hard constraints in the inner subproblem. This separation preserves the MPCC structure and avoids the pathological multiplier growth that can arise when complementarity conditions are penalized directly [16, 15]. The resulting AuLa subproblem, with objective denoted by $\Phi(X, Y, Z)$, is

$$\min_{X,Y,Z} \frac{1}{2} \sum_{t=1}^T r_t^\top r_t + \frac{\rho_{\bar{h}}}{2} \left\| \bar{h}_t + \frac{\kappa_t}{\rho_{\bar{h}}} \right\|^2 + \frac{\rho_g}{2} \left\| (g_t + \frac{\mu_t}{\rho_g})_+ \right\|^2 \quad (4a)$$

$$\text{s.t. } 0 \leq y_t \perp z_t \geq 0, \quad t \in \{1, \dots, T\}. \quad (4b)$$

For brevity, we omit explicit dependence on the variables and stack the equality constraints in (3) at time step t as $\bar{h}_t(x_t, x_{t+1}, y_t, z_t) := [h(x_t, x_{t+1}); G(x_t) - y_t; H(x_t) - z_t]$. At the terminal time step $t = T$, $\bar{h}_t(x_t, x_{t+1})$ reduces to $h(x_t)$, as no dynamics constraint is imposed beyond the terminal state. The operator $(\cdot)_+$ denotes the element-wise positive part, $(x)_+ := \max(x, 0)$. We use $\rho_{\bar{h}}$ and ρ_g as penalty factors for the equality and inequality constraints, with corresponding multipliers κ_t and μ_t . The resulting subproblem (4) is a

Algorithm 1 Safeguarded AuLa outer loop for MPCCs

Require: Initial multipliers (κ^0, μ^0) , penalties $(\rho_{\bar{h}}^0, \rho_g^0)$, safeguard bounds $\mu_{\max} > 0$ and $\kappa_{\min} < \kappa_{\max}$, penalty increase factor $\gamma > 1$, constraints violation factor $\eta \in [0, 1]$, inner problem tolerances $\{\varepsilon_k\} \downarrow 0$, outer problem tolerances $\epsilon_w, \epsilon_g, \epsilon_{\bar{h}}$.

- 1: Initialize w^0
- 2: Set $k \leftarrow 0$. Initial variable-change $\|\Delta w^0\|_\infty \leftarrow \infty$.
- 3: **while** $\|\Delta w^k\|_\infty \geq \epsilon_w$ or $\|(g(X^k))_+\|_\infty \geq \epsilon_g$ or $\|\bar{h}(w_k)\|_\infty \geq \epsilon_{\bar{h}}$ **do**
- 4: **Safeguard multipliers:**

$$\bar{\kappa}^k \leftarrow \Pi_{[\kappa_{\min}, \kappa_{\max}]}(\kappa^k), \quad \bar{\mu}^k \leftarrow \Pi_{[0, \mu_{\max}]}(\mu^k),$$

where Π denotes component-wise clipping.

- 5: **Inner solve:** approximately solve the AuLa subproblem (4) with $\bar{\mu}^k, \bar{\kappa}^k$ and obtain $w^{k+1} = (X^{k+1}, Y^{k+1}, Z^{k+1})$ such that the inner stationary residual is below ε_k .

- 6: Evaluate \bar{h}_t, g_t using w^{k+1} , $\Delta w^k \leftarrow w^{k+1} - w^k$

- 7: **Multiplier update:**

$$\kappa^{k+1} \leftarrow \bar{\kappa}^k + \rho_{\bar{h}}^k \bar{h}_t, \quad \mu_t^{k+1} \leftarrow (\bar{\mu}_t^k + \rho_g^k g_t)_+,$$

- 8: $\zeta_t^{k+1} \leftarrow \min(\mu_t^{k+1}, -g_t)$

- 9: **Penalty update:**

- 10: **if** $k = 0$ or $\max\{\|\zeta^{k+1}\|_\infty, \|\bar{h}(w^{k+1})\|_\infty\} \leq$

$\eta \max\{\|\zeta^k\|_\infty, \|\bar{h}(w^k)\|_\infty\}$ **then**

- 11: $\rho_{\bar{h}}^{k+1} \leftarrow \rho_{\bar{h}}^k; \rho_g^{k+1} \leftarrow \rho_g^k$.

- 12: **else**

- 13: $\rho_{\bar{h}}^{k+1} \leftarrow \gamma \rho_{\bar{h}}^k; \rho_g^{k+1} \leftarrow \gamma \rho_g^k$.

- 14: **end if**

- 15: $k \leftarrow k + 1$.

- 16: **end while**
-

nonlinear least-squares problem with simple complementarity constraints.

To promote global convergence of the outer loop, we use the safeguarded multiplier and penalty updates in Algorithm 1. Updates are applied component-wise across all time steps, and multipliers are clipped to fixed safeguard bounds to ensure they remain bounded. Lines 8–14 implement a standard safeguard for penalty updates: we monitor the decrease of the equality-feasibility residual $\|\bar{h}(w^{k+1})\|_\infty$ and an inequality complementarity/KKT residual $\|\zeta^{k+1}\|_\infty$ computed after the multiplier update; if the combined violation does not decrease sufficiently, we increase the penalty parameters. This is one possible safeguard design, and other update rules that enforce a comparable sufficient-decrease condition can be used as well.

The accuracy of each inner solve directly affects the convergence behavior of the AuLa outer loop. To formalize this connection, we introduce a computable KKT residual for the AuLa subproblem (4) and use it as the inner-solve accuracy criterion in line 5 of Algorithm 1. This residual verifies: (i) stationarity of the augmented objective, (ii) feasibility of the complementarity set $0 \leq Y \perp Z \geq 0$, and (iii) consistency of

the complementarity multipliers with the limiting normal cone of this set. The full definition of the KKT residual is given in Appendix A.

Definition 2 (ϵ -stationarity). At outer iteration k , let Φ^k denote the AuLa objective in (4) with safeguarded multipliers and penalty factors. We say $w^k = (X^k, Y^k, Z^k)$ is ϵ -stationary for (4) if

$$r_{\text{in}}(w^k) \doteq \inf_{(u,v) \in \mathcal{M}_M(w^k)} r_{\text{in}}(w^k; u, v) \leq \epsilon,$$

where r_{in} is computed with respect to Φ^k , and $\mathcal{M}_M(w^k)$ is the branch-dependent multiplier set defined in Appendix A.

The residual r_{in} is chosen so that the inner and outer accuracy criteria are consistent. It gives a computable certificate for the AuLa subproblem and is compatible with the gradient-mapping measure controlled by the inner solver introduced later in Section V. Therefore, the condition $r_{\text{in}} \leq \epsilon$ is both the accuracy requirement used by the safeguarded AuLa analysis and a natural stopping measure for the inner routine. The formal statement and assumptions are deferred to Appendix B.

We rephrase the global convergence/stationarity result of [16, Thm. 3] (and the closely related statement in [15, Cor. 4.4]) in terms of the KKT residual:

Theorem 3 (Global convergence of safeguarded AuLa under vanishing inner residual). Let $\{w^k\}$ be the sequence generated by Algorithm 1. Assume that the safeguarded multipliers $(\bar{\kappa}^k, \bar{\mu}^k)$ remain bounded (e.g., line 4 of Algorithm 1). Suppose the AuLa subproblem (4) is solved inexactly in the sense that, for each k , there exist (u^k, v^k) such that

$$r_{\text{in}}(w^k; u^k, v^k) \leq \epsilon_k, \quad \epsilon_k \downarrow 0.$$

Let w^* be a feasible accumulation point of $\{w^k\}$ for (3) (equivalently, for (1)). If the MPCC regularity condition assumed in [16, Thm. 3] holds at w^* , then w^* is a first-order stationary point of the MPCC (in the sense of [16, Thm. 3]).

Therefore, to ensure the *attainability* of stationarity, we design an inner solver to meet the Definition 2 for any prescribed tolerance $\epsilon > 0$ within finitely many inner iterations. We present such a solver in the next section.

V. A BCD INNER SOLVER FOR AU LA SUBPROBLEMS

We solve the AuLa inner subproblem (4) with a two-block coordinate descent (BCD) scheme. Each BCD iteration alternates between updating the trajectory variables X and updating the auxiliary complementarity variables (Y, Z) . The X -update is carried out by a Gauss-Newton update with globalization, and the (Y, Z) -update admits a closed-form solution under the complementarity constraints.

a) Block 1: X -update (Gauss-Newton with globalization): With (Y, Z) fixed, the inner objective reduces to a smooth nonlinear least-squares problem in X . We solve it using a damped Gauss-Newton method with an Armijo backtracking line search to ensure sufficient decrease of the inner objective Φ^k .

b) Block 2: (Y, Z) -update (closed-form minimization over a union of cones): With X fixed, the (Y, Z) -subproblem decouples across time steps and complementary pairs. For i th scalar pair at time t : $(y_{t,i}, z_{t,i})$ subject to $0 \leq y_{t,i} \perp z_{t,i} \geq 0$, the feasible set is the union of two convex cones, $\mathcal{C} = \{(y, 0) \mid y \geq 0\} \cup \{(0, z) \mid z \geq 0\}$. Thus we evaluate two closed-form candidates and select the one yielding the smaller quadratic penalty contribution in (4).

With the safeguarded multipliers at outer iteration k and current penalty factor $\rho_{\bar{h}}$:

Case 1 ($z_{t,i} = 0$):

$$y_{t,i}^* = \max\left(0, G_i(x_t) + \frac{1}{\rho_{\bar{h}}} \kappa_{G,t,i}\right), \quad z_{t,i}^* = 0. \quad (5)$$

Case 2 ($y_{t,i} = 0$):

$$z_{t,i}^* = \max\left(0, H_i(x_t) + \frac{1}{\rho_{\bar{h}}} \kappa_{H,t,i}\right), \quad y_{t,i}^* = 0. \quad (6)$$

We then pick between (5) and (6) by comparing their resulting objective values (equivalently, their quadratic penalty contributions). This step is an *exact* minimization over the complementarity set for fixed X and hence never increases Φ^k . We summarize the BCD approach as Algorithm 2. A graphical depiction of the algorithm is shown in Fig. 2.

Remark 4 (Why this differs from the ADMM projection in [30]). The ADMM projection in [30] is primarily feasibility-driven in consensus step: it directly projects the copied variable onto the complementarity-feasible set. In contrast, our closed-form update corresponds to a *shifted* mapping induced by the current approximate Lagrange multipliers and penalty weights. Unlike an ADMM consensus update, this step does not introduce copied variables; it is obtained by directly minimizing the AuLa subproblem with respect to the slack variables. This mapping injects the influence of the current multiplier/penalty into the slack variables, acting like a spring force that regularizes the primal update. As illustrated in Fig. 2, IMPACT therefore provides more than a pure feasibility projection and can yield substantially faster progress.

Theorem 5 (Attainability of ϵ -stationarity by the BCD inner solver). Fix an outer iteration k and consider the BCD inner iterates $\{w^{(j)}\} = \{(X^{(j)}, Y^{(j)}, Z^{(j)})\}$ generated by Algorithm 2. Assume: (i) Φ^k is continuously differentiable, $\nabla \Phi^k$ is Lipschitz on the bounded set visited by the iterates and Φ^k is bounded below on $\{(X, Y, Z) : (Y, Z) \in \mathcal{C}\}$; (ii) the X -update is globalized and achieves sufficient decrease (e.g., damped GN with Armijo line search); and (iii) the (Y, Z) -update is an exact minimization over the complementarity set for fixed X (as in (5)–(6)). Then, for any tolerance $\epsilon_k > 0$, there exists a finite inner iteration index j_k and multipliers $(u^{(j_k)}, v^{(j_k)})$ such that

$$r_{\text{in}}(w^{(j_k)}; u^{(j_k)}, v^{(j_k)}) \leq \epsilon_k.$$

In particular, the inner BCD loop can be terminated after finitely many iterations with an output w^k that is ϵ_k -stationary in the sense of Definition 2.

Algorithm 2 Inner Solver: BCD for the AuLa subproblem (4)

Require: Outer index k , safeguarded multipliers $(\bar{\kappa}^k, \bar{\mu}^k)$, penalties (ρ_h^k, ρ_g^k) , initial $(X^{(0)}, Y^{(0)}, Z^{(0)})$, stagnation tolerance τ_k

- 1: Set $w^{(0)} \leftarrow (X^{(0)}, Y^{(0)}, Z^{(0)})$ and evaluate $\Phi^k(w^{(0)})$.
- 2: **for** $j = 0, 1, 2, \dots$ **do**
- 3: **X-update:** compute a damped GN update on $\Phi^k(\cdot, Y^{(j)}, Z^{(j)})$ with backtracking line search; obtain $X^{(j+1)}$.
- 4: **(Y, Z)-update:** for each (t, i) , compute candidates (5) and (6) and select the one with smaller objective; obtain $(Y^{(j+1)}, Z^{(j+1)})$.
- 5: Set $w^{(j+1)} \leftarrow (X^{(j+1)}, Y^{(j+1)}, Z^{(j+1)})$ and evaluate $\Phi^k(w^{(j+1)})$.
- 6: **Practical stopping:** if $|\Phi^k(w^{(j)}) - \Phi^k(w^{(j+1)})| \leq \tau_k$,
- 7: **return** $w^k \leftarrow w^{(j+1)}$.
- 8: **end for**

The proof is given in Appendix B: sufficient decrease makes the X -block residual attainable, and exact (Y, Z) -minimization eliminates the complementarity-block part of the KKT residual.

Inner-solver guarantee and practical stopping. The inner optimizer is *not* intended to certify global optimality of the nonconvex subproblem. For the purpose of *outer-loop convergence analysis*, we adopt an *attainability* interface: for any tolerance $\varepsilon > 0$, the inner procedure can produce (in finitely many iterations) an iterate whose stationarity measure is below ε under suitable multipliers (Theorem 5). Our implementation, however, uses an *inexact/budgeted* inner solve: we do not explicitly test stationarity and instead stop when the inner augmented objective stagnates, $|\Phi^k(w^{(j)}) - \Phi^k(w^{(j+1)})| \leq \tau_k$. Empirically, this criterion consistently yields sufficiently small constraint and complementarity residuals and stable outer-loop progress on all benchmarks; see Appendix B for definitions and additional diagnostics.

VI. EXPERIMENTS

In this section, we evaluate our planner on two open-source benchmarks. For long-horizon planning, we use the CITO benchmark from CRISP [11]. For dexterous manipulation under multi-contact dynamics, we use the CI-MPC benchmark from [13]. All experiments are run on a desktop PC with an AMD Ryzen 9 7950X3D CPU, with no GPU acceleration. Our IMPACT implementation uses no explicit multi-threading (e.g., OpenMP/TBB). It links against BLAS/LAPACK, uses Eigen’s sparse LDLT factorization for linear solves, and updates slack pairs using Eigen’s SIMD-vectorized operations. We use CasADi’s C++ interface for modeling and symbolic differentiation [34]. CasADi CodeGen is disabled for both CITO and CI-MPC.

A. Long Horizon CITO Benchmark

The CRISP CITO benchmark comprises six nonlinear, hybrid-dynamics, contact-rich problems for long-horizon plan-

ning. The CRISP paper compares standard NLP solvers on four tasks. We exclude the one task that requires a manually specified initial guess, which is outside our scope, and evaluate on three tasks: Push Box, Cart Transport, and Push T.

Rather than comparing against generic NLP solvers that do not explicitly handle complementarity constraints and are often brittle on MPCCs (e.g., SNOPT and PROXNLP [11]), we compare against solution strategies that are known to perform well in practice: **Scholtes relaxation (SR)**, the square **penalty method (PM)**, and **CRISP**. To handle the long planning horizons in these benchmarks, we formulate all evaluated methods using multiple shooting. We implement SR and PM using the IPOPT C++ interface [35], with symbolic automatic differentiation provided by the CasADi C++ interface. For **CRISP**, we directly use the released C++ implementation provided by the authors, which is specialized to the benchmark problems.

For **SR**, we enforce the nonnegativity constraints $G(x) \geq 0$ and $H(x) \geq 0$ explicitly as inequalities, which IPOPT handles reliably, and relax complementarity via $G(x)H(x) \leq t$. We then solve a sequence of relaxed problems, initialized with $t = 1.0$ and reducing t by a factor of 10 at each outer iteration until $t = 10^{-10}$. In our experiments, this continuation schedule provides a robust trade-off between numerical stability and runtime. The outer loop terminates early when the complementarity residual falls below a prescribed tolerance. For efficiency, we warm-start IPOPT using the previous iterate’s primal and dual variables.

For **PM**, we keep $G(x) \geq 0$ and $H(x) \geq 0$ as explicit inequality constraints and penalize complementarity using a squared penalty term with a relatively large penalty weight. Empirically, this configuration is stable and often more efficient than starting from a small penalty and gradually increasing it. While a large penalty can make the inner NLP more ill-conditioned, we find IPOPT remains effective in this regime and can be more efficient than an iterative NLP scheme.

The benchmark problems are shown in Fig. 3, and we provide detailed descriptions in Appendix C. We remark that these tasks require forward integration of nonlinear dynamics and include general equality and inequality constraints, so they are not directly cast as LCPs solvable by standard LCP solvers. We report problem sizes in terms of decision variables, complementarity pairs, and constraint counts: *Push Box* has 453 variables, 500 complementarity pairs, and 150 dynamics constraints. *Push T* has 1353 variables, 2150 complementarity pairs, 150 dynamics constraints, 350 equality constraints, and 200 inequality constraints. *Cart Transport* has 2404 variables, 900 complementarity pairs, 1200 dynamics constraints, 300 equality constraints, and 1200 inequality constraints.

Solver Settings and Performance Metrics: We use an all-zero initialization for every solver on all tasks, following the standardized CRISP comparison setup. This choice avoids task-specific initial guesses and makes the comparison reproducible across methods. We note, however, that warm-started initialization is common in practical TO/MPC pipelines, and the relative advantage of IMPACT may differ in such settings.

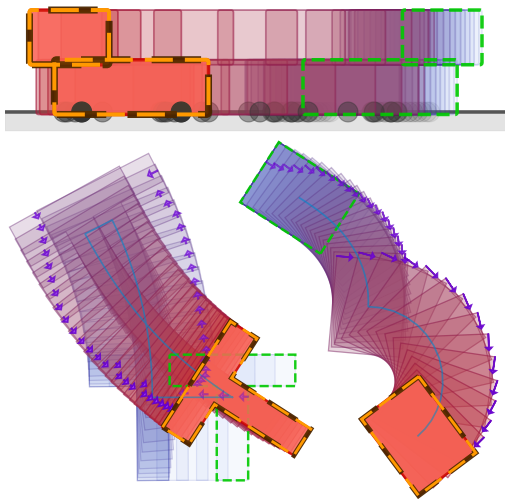


Fig. 3: IMPACT planning demos on three CITO tasks. The green dashed box marks the start pose and the orange dashed box marks the goal pose. Purple arrows visualize contact forces, and the solid green line traces the object-origin trajectory. Color indicates time from early (light blue) to late (dark orange).

For each task, all methods (SR/PM/IMPACT and CRISP) are synchronized to solve the same optimization problem with identical objective-function weights. For *Push Box* and *Push T*, we use a horizon of $T = 50$ with $\Delta t = 0.05$; for *Cart Transport*, we use $T = 300$ with $\Delta t = 0.02$. For *Push Box* and *Push T*, we randomly sample 50 goal poses, and for *Cart Transport*, we randomly sample 50 start-goal pairs.

We run each planner until it satisfies a common set of termination criteria. Specifically, we require all constraint violations to be below 10^{-5} , including (for example) the complementarity violation $\|G(x) \circ H(x)\|_{\infty} \leq 10^{-5}$. A run is declared a failure if (i) it reaches the maximum iteration limit (2000 in our experiments) while still violating either stopping criterion, or (ii) the resulting trajectory fails to reach the goal (e.g., becoming stuck in an intermediate configuration), a failure mode also reported in the CRISP paper. Otherwise, the run is counted as successful. We report success rate, total tracking error, iteration count, and wall-clock runtime in Table I. We report total tracking error as an end-to-end task metric; lower values typically indicate trajectories that reach the goal sooner and maintain better tracking, which often correlates with more efficient contact-mode progress. For IMPACT, we report the number of BCD sweeps, where one sweep corresponds to a full pass over all blocks. For CRISP, we report the total number of QP solves (including those from second-order corrections) as the subproblem-count metric. The MPCC formulations and all solver hyperparameters are provided in Appendix C.

Table I shows a quality-speed trade-off across solvers. In terms of *model/trajectory quality* (total tracking error), SR is best on *Push Box* and *Push T*, while CRISP is best on *Cart Transport*. IMPACT remains competitive: it is second-best on *Push Box* and *Cart Transport*, and close to CRISP

TABLE I: CITO benchmark results reported as mean \pm 95% confidence interval (CI). For each task and metric, the best method is highlighted in **red** and the second best in **blue**.

Task	Solver	Success (%)	Track. Err. \downarrow	Iters \downarrow	Time (s) \downarrow
<i>Box</i>	SR	100.0	19.46 \pm 2.30	164 \pm 12	1.27 \pm 0.10
	PM	98.0	58.00 \pm 5.11	66 \pm 13	0.85 \pm 0.17
	CRISP	100.0	51.90 \pm 4.08	641 \pm 358	2.52 \pm 1.34
	IMPACT	100.0	26.99 \pm 2.81	219 \pm 49	0.15 \pm 0.03
<i>T</i>	SR	100.0	1.24 \pm 0.13	202 \pm 11	5.50 \pm 0.38
	PM	90.0	21.99 \pm 2.57	117 \pm 14	2.96 \pm 0.39
	CRISP	100.0	8.03 \pm 0.71	1243 \pm 407	25.73 \pm 6.92
	IMPACT	100.0	8.48 \pm 1.94	606 \pm 225	1.03 \pm 0.44
<i>Cart</i>	SR	100.0	433.08 \pm 44.92	261 \pm 22	5.63 \pm 0.57
	PM	100.0	408.65 \pm 42.32	87 \pm 14	2.00 \pm 0.32
	CRISP	100.0	235.10 \pm 21.70	501 \pm 381	2.72 \pm 2.05
	IMPACT	100.0	381.89 \pm 32.35	101 \pm 15	0.08 \pm 0.01

on *Push T*. In contrast, PM yields the largest tracking errors and is also less robust, with failures on *Push T* (90% success) and *Push Box* (98% success). In terms of *efficiency*, IMPACT provides a dominant runtime advantage. Despite PM having fewer iterations, the penalized subproblems can be ill-conditioned, so wall-clock time does not scale with iteration count. We find that driving the complementarity violation down to the 10^{-5} level typically requires multiple continuation iterations in CRISP, leading to increased runtime. SR also remains comparatively expensive, as we find that warm-starting does not substantially reduce the iteration count in practice. Quantitatively, IMPACT is 16.8 \times , 25.0 \times , and 34.0 \times faster than CRISP on *Box*, *T*, and *Cart*, respectively (geometric mean 24.3 \times). Even relative to the fastest baseline in time (PM), IMPACT achieves 5.7 \times , 2.9 \times , and 25.0 \times speedups (geometric mean 7.4 \times). Across all baseline comparisons in Table I, this corresponds to a 2.9 \times –70 \times speedup range with a geometric mean of 13.8 \times .

B. Real-Robot Push-T Demonstration

To evaluate IMPACT beyond simulation, we deploy it on a real robotic pushing setup for the Push-T task as a qualitative hardware demonstration (Fig. 1). We first solve a full-horizon TO problem to obtain a reference pushing trajectory, and then execute it on the robot by commanding the end-effector to emulate the pusher and track the reference. If the object deviates too much from the nominal trajectory, we replan online. To improve sim-to-real fidelity, we tune the rotational *contact-radius* constraint in the contact model based on observed rollouts. We run 10 trials with different initial object configurations; IMPACT reaches the target in all trials, achieving a 100% success rate. Additional videos are provided in the supplementary material.

C. Multi-contact High Dimensional CI-MPC Benchmark

To evaluate the scalability of IMPACT in a realistic CI-MPC setting, we use the Allegro Hand meshable-object re-orientation benchmark introduced in [13]. Following [13], we refer to the overall evaluation setup under their framework as

Success (%)	IMPACT	80	100	90	100	90	100	80	100	100	100	100	90	100	30	100	100	100	91.8±4.1
	C-Free (0.1)	90	70	100	100	50	100	100	100	90	100	100	100	100	50	100	100	100	91.2±4.2
	C-Free (0.2)	100	80	100	100	60	100	90	100	90	100	100	90	100	70	100	100	100	92.9±3.9
Ctrl Var	IMPACT	1.97	1.49	1.59	1.16	1.78	1.49	1.53	1.29	1.36	1.58	1.66	1.96	1.69	1.63	1.27	1.79	1.08	1.55±0.13
	C-Free (0.1)	2.60	2.47	2.32	1.90	2.26	1.50	2.28	1.77	2.24	1.85	2.20	2.34	2.45	2.46	2.47	2.44	1.09	2.16±0.21
	C-Free (0.2)	5.28	4.62	5.15	3.35	5.00	3.03	4.62	4.75	4.78	3.75	3.76	5.50	5.15	5.65	4.51	4.50	2.11	4.44±0.49
Smooth	IMPACT	0.045	0.027	0.032	0.018	0.035	0.022	0.028	0.015	0.024	0.032	0.034	0.042	0.034	0.031	0.022	0.039	0.018	0.029±0.004
	C-Free (0.1)	0.060	0.046	0.045	0.045	0.036	0.018	0.051	0.026	0.046	0.033	0.037	0.043	0.051	0.051	0.070	0.071	0.014	0.044±0.008
	C-Free (0.2)	0.109	0.121	0.106	0.072	0.077	0.045	0.099	0.108	0.103	0.067	0.067	0.097	0.086	0.090	0.112	0.097	0.035	0.088±0.012
Effort	IMPACT	4.8	4.0	1.7	1.7	2.3	2.6	6.0	1.6	2.0	4.1	2.0	1.9	1.6	8.7	1.7	3.5	1.2	3.0±1.0
	C-Free (0.1)	6.3	5.7	2.0	2.1	12.5	4.5	5.7	2.0	2.4	1.8	3.4	6.4	3.6	15.2	2.1	3.7	1.4	4.8±2.0
	C-Free (0.2)	9.5	3.2	6.3	3.3	12.2	10.3	17.9	4.6	3.5	3.0	4.0	5.0	6.7	40.4	3.4	4.2	1.9	8.2±4.8
		Airpl	Binoc	Bowl	Bunny	Camr	Can	Cube	Cup	Eleph	Foamb	Mug	Piggy	Rubbe	Stick	Teapo	Torus	Water	Avg



Fig. 4: Allegro-Hand CI-MPC benchmark results on 17 objects. We compare IMPACT against *cfree*(0.1) and *cfree*(0.2), which use control bounds $[-0.1, 0.1]$ and $[-0.2, 0.2]$, respectively. Reported metrics include **success rate (Success)** and control-quality measures: control variance (**Ctrl Var**), control smoothness (**Smooth**), and control effort (**Effort**). Table columns use these abbreviations. For each object, the best value for each metric is highlighted, and the final column reports the aggregate results with a 95% confidence region across all 17 objects.

cfree in the remainder of the paper. As a point of reference, the *cfree* pipeline relies on **smoothing-based** contact modeling together with the interior-point NLP solver IPOPT, and achieves a 50-60 Hz CI-MPC on our test PC. However, smoothing-based CI-MPC can exhibit undesired closed-loop behavior: smoothed contact transitions may degrade control smoothness and induce oscillations during execution. In contrast, our goal in this experiment is to demonstrate that IMPACT scales to this benchmark and achieves a practically useful control rate of around 10 Hz on the same hardware. Importantly, this rate is achieved while directly solving a *multi-contact, nonsmooth, MPCC-based* MPC problem *without* smoothing or relaxation. Such problems are widely considered challenging for real-time control due to the combinatorial mode structure and nonsmooth contact dynamics.

The *cfree* benchmark includes 17 objects spanning a wide range of surface curvatures and shapes; see Fig. 4 for the object set. The Allegro-hand setup can involve up to 20 simultaneous detected contact points; the contact complementarity conditions below are instantiated for each detected contact. We adhere closely to the *cfree* setup and keep all hyperparameters unchanged, including (but not limited to) the simulation time step, friction coefficients, and inertial parameters. The full list of parameters is provided in Appendix C.

In IMPACT, we optimize over the generalized velocities \mathbf{v}_t , contact forces β_t and control \mathbf{u}_t ; given the relatively short MPC horizon, we use a single-shooting formulation and eliminate the position states by forward integration. The MPC horizon matches *cfree* and is set to 4. Following *cfree*, we compute the contact Jacobian only at the MPC initial state and hold it fixed over the prediction horizon.

We keep the same objective structure as *cfree*, but replace its quaternion inner-product term with a log-map rotation residual in \mathbb{R}^3 , yielding a standard nonlinear least-squares form that better matches our Gauss-Newton pipeline. To keep the relative influence of the rotation terms comparable, we increase its weight accordingly. To improve closed-loop damping, we additionally include a small penalty on object velocity; in contrast, *cfree* primarily introduces damping via

penalties on contact forces expressed in the contact frame. We do not perform per-object tuning: as in *cfree*, we use a single shared set of control parameters across all 17 objects. For initialization, we follow the same strategy as *cfree* by adding small random perturbations to the object’s start and goal poses in hand. We also adopt the same success criteria as *cfree*: a squared position-norm error below 0.02 and a quaternion inner-product error below 0.04. Each object is evaluated over 10 trials. The total simulation horizon is 1000 time steps with a time step of 0.1 s. One key difference from the default *cfree* setup is the control bound: we use $[-0.1, 0.1]$ to promote a locally stable contact mode. For comparison, we also report *cfree* results with control bounds $[-0.1, 0.1]$ and $[-0.2, 0.2]$. Our IMPACT experiments use MuJoCo’s C API via a C++ interface to match our optimizer implementation, whereas we run *cfree* using its released Python implementation. The experimental results are reported in Fig. 4. Besides the success rate, we report three control-quality metrics. Control variance is defined as $\frac{1}{d} \sum_{i=1}^d \text{Var}(\mathbf{b}_i)$, where d is the dimension of the control signal. Control smoothness is computed as $\frac{1}{T-2} \sum_{t=1}^{T-2} \|\mathbf{u}_{t+1} - \mathbf{u}_t\|_2^2$, and control effort as $\sum_{t=1}^{T-1} \|\mathbf{u}_t\|_2^2$, where T is the trial length.

Fig. 4 summarizes performance across the 17 objects. IMPACT achieves a success rate comparable to *cfree* (avg. $91.8\% \pm 4.1$ vs. $91.2\% \pm 4.2$ for *cfree*(0.1) and $92.9\% \pm 3.9$ for *cfree*(0.2)), while consistently improving control quality: variance 1.55 ± 0.13 (vs. 2.16 ± 0.21 and 4.44 ± 0.49), smoothness 0.029 ± 0.004 (vs. 0.044 ± 0.008 and 0.088 ± 0.012), and effort 3.0 ± 1.0 (vs. 4.8 ± 2.0 and 8.2 ± 4.8) for *cfree*(0.1/0.2) [13]. Increasing *cfree*’s control bound from $[-0.1, 0.1]$ to $[-0.2, 0.2]$ preserves success rate but substantially worsens these control-quality metrics, consistent with more oscillatory closed-loop behavior under aggressive inputs. The *stick* object is a notable outlier where IMPACT performs worse; we attribute this to the heightened sensitivity of long, slender geometries to LCP-based contact modeling, which can induce frequent mode switching. In terms of efficiency, IMPACT completes successful trials in 66.5 ± 10.9 MPC steps, comparable to *cfree*(0.1) 71.4 ± 13.5 and *cfree*(0.2) 57.8 ± 14.6 , but runs

at a lower control rate of 9.53 ± 0.36 Hz (vs. 50.6 ± 0.86 and 54.0 ± 1.30 Hz).

VII. LIMITATIONS

a) *Contact-mode stability under limited compute:* In the Allegro-hand CI-MPC experiments, we observe a transient regime before contact is firmly established in which the optimizer may switch between nearby contact sets. This behavior is most pronounced under tight real-time compute budgets, where only coarse inner solves are feasible and the contact-branch selections can vary across iterations. Despite this, IMPACT scales well to high-dimensional MPCC-based CI-MPC and achieves strong aggregate performance on the benchmark. Incorporating additional stabilization mechanisms (e.g., trust-region [36] or hysteresis on mode updates) is a promising direction to further reduce contact-set switching in this regime.

b) *Local planning and dependence on contact-encouraging costs:* Under a limited compute budget, IMPACT in the Allegro-hand setup operates as a local planner. While it is effective and yields smooth behavior in many cases, it can be sensitive to local minima and depends on a contact-encouraging cost adopted from [13]. This limitation is most visible on the stick object, where slender geometry makes contact maintenance highly sensitive. Such heuristic contact terms can increase sensitivity to hyperparameters and contribute to residual oscillations; the smoother Push-T results suggest that global geometric encodings can reduce this reliance. Promising directions include incorporating offline reinforcement learning to provide global guidance and reduce reliance on hand-crafted contact costs, as well as exploring object representations beyond local parameterizations to improve robustness. We leave these directions to future work.

VIII. CONCLUSION

We presented IMPACT, an implicit contact active-set augmented Lagrangian method for fast contact-implicit trajectory optimization. IMPACT combines a safeguarded AuLa outer loop for MPCCs with a structured block coordinate descent inner solver, enabling efficient contact-mode discovery without a prescribed continuation schedule while retaining the original nonsmooth complementarity structure.

We implemented IMPACT in C++ and evaluated it on two open-source benchmarks. On the CRISP long-horizon CITO suite, IMPACT achieves substantial runtime gains over strong baselines, with speedups ranging from $2.9\times$ to $70\times$ (geometric mean $13.8\times$). In particular, compared with CRISP, IMPACT is $16.8\times$, $25.0\times$, and $34.0\times$ faster on Push Box, Push T, and Cart Transport, respectively (geometric mean $24.3\times$), while maintaining competitive task-level tracking performance under the same feasibility/stationarity termination criteria.

On the high-dimensional multi-contact CI-MPC benchmark for dexterous manipulation, we demonstrate that the proposed IMPACT architecture scales beyond offline planning to closed-loop control. IMPACT scales to multi-contact dynamics in generalized coordinates and, at comparable success rates

to the baseline, yields improved control-quality metrics (lower control variance/smoothness/effort). Finally, we demonstrate the proposed method on real robotic hardware in a Push-T manipulation task.

ACKNOWLEDGMENTS

This work was supported by the DFG Emmy Noether Programme (CH 2676/1-1), the EU Horizon Europe projects MANiBOT (101120823) and ARISE (101135959), the BMFTR project RIG (16ME1001), and the ERC project SIREN (101163933). We also acknowledge support from the hessian.AI Service Center (BMFTR, 16IS22091), the hessian.AI Innovation Lab (S-DIW04/0013/003), TAM, RAI, Google, and the Alfried Krupp Foundation.

REFERENCES

- [1] Karim Bouyarmane, Stéphane Caron, Adrien Escande, and Abderrahmane Kheddar. Multi-contact motion planning and control. In Amit Goswami and Prahlad Vadakkepat, editors, *Humanoid Robotics: A Reference*. Springer Nature, 2019. doi: 10.1007/978-94-007-6046-2_32.
- [2] Tao Pang, HJ Terry Suh, Lujie Yang, and Russ Tedrake. Global planning for contact-rich manipulation via local smoothing of quasi-dynamic contact models. *IEEE Transactions on Robotics*, 39(6):4691–4711, 2023.
- [3] Wilson Jallet, Antoine Bambade, Etienne Arlaud, Sarah El-Kazdadi, Nicolas Mansard, and Justin Carpentier. Proxddd: Proximal constrained trajectory optimization. *IEEE Transactions on Robotics*, 2025.
- [4] Carlos Mastalli, Rohan Budhiraja, Wolfgang Merkt, Guilhem Saurel, Bilal Hammoud, Maximilien Naveau, Justin Carpentier, Ludovic Righetti, Sethu Vijayakumar, and Nicolas Mansard. Crocodyl: An efficient and versatile framework for multi-contact optimal control. In *Proc. IEEE International Conference on Robotics and Automation (ICRA)*, 2020.
- [5] Michael Posa, Cecilia Cantu, and Russ Tedrake. A direct method for trajectory optimization of rigid bodies through contact. *The International Journal of Robotics Research*, 33(1):69–81, 2014.
- [6] Aykut Özgün Öno, Philip Long, and Taşkın Padır. Contact-implicit trajectory optimization based on a variable smooth contact model and successive convexification. In *2019 International Conference on Robotics and Automation (ICRA)*, pages 2447–2453. IEEE, 2019.
- [7] Jean-Pierre Sleiman, Farbod Farshidian, and Marco Hutter. Versatile multicontact planning and control for legged loco-manipulation. *Science Robotics*, 8(81):eadg5014, 2023. doi: 10.1126/scirobotics.adg5014.
- [8] Quentin Le Lidec, Wilson Jallet, Louis Montaut, Ivan Laptev, Cordelia Schmid, and Justin Carpentier. Contact models in robotics: a comparative analysis. *IEEE Transactions on Robotics*, 2024.
- [9] Holger Scheel and Stefan Scholtes. Mathematical programs with complementarity constraints: Stationarity,

- optimality, and sensitivity. *Mathematics of Operations Research*, 25(1):1–22, 2000.
- [10] Armin Nurkanović, Anton Pozharskiy, and Moritz Diehl. Solving mathematical programs with complementarity constraints arising in nonsmooth optimal control: A. nurkanović et al. *Vietnam Journal of Mathematics*, 53(3):659–697, 2025.
- [11] Yulin Li, Haoyu Han, Shucheng Kang, Jun Ma, and Heng Yang. On the Surprising Robustness of Sequential Convex Optimization for Contact-Implicit Motion Planning. In *Proceedings of Robotics: Science and Systems*, Los Angeles, CA, USA, June 2025. doi: 10.15607/RSS.2025.XXI.047.
- [12] Vince Kurtz, Alejandro Castro, Aykut Özgün Önel, and Hai Lin. Inverse dynamics trajectory optimization for contact-implicit model predictive control. *The International Journal of Robotics Research*, 45(1):23–40, 2026.
- [13] Wanxin Jin. Complementarity-Free Multi-Contact Modeling and Optimization for Dexterous Manipulation. In *Proceedings of Robotics: Science and Systems*, Los Angeles, CA, USA, June 2025. doi: 10.15607/RSS.2025.XXI.111.
- [14] Sotaro Katayama, Tatsunori Tani, and Kazutoshi Tanaka. Quasistatic contact-rich manipulation via linear complementarity quadratic programming. In *2022 IEEE/RSJ International Conference on Intelligent Robots and Systems (IROS)*, pages 203–210. IEEE, 2022.
- [15] Xiaoxi Jia, Christian Kanzow, Patrick Mehlitz, and Gerd Wachsmuth. An augmented lagrangian method for optimization problems with structured geometric constraints. *Mathematical Programming*, 199(1):1365–1415, 2023.
- [16] Lei Guo and Zhibin Deng. A new augmented lagrangian method for mpc—theoretical and numerical comparison with existing augmented lagrangian methods. *Mathematics of Operations Research*, 47(2):1229–1246, 2022.
- [17] Alberto De Marchi, Xiaoxi Jia, Christian Kanzow, and Patrick Mehlitz. Constrained composite optimization and augmented lagrangian methods. *Mathematical Programming*, 201(1):863–896, 2023.
- [18] Christian Kanzow and Patrick Mehlitz. Convergence properties of monotone and nonmonotone proximal gradient methods revisited. *Journal of Optimization Theory and Applications*, 195(2):624–646, 2022.
- [19] Hyung Ju Terry Suh, Tao Pang, and Russ Tedrake. Bundled gradients through contact via randomized smoothing. *IEEE Robotics and Automation Letters*, 7(2):4000–4007, 2022.
- [20] Simon Le Cleac’h, Taylor A Howell, Shuo Yang, Chi-Yen Lee, John Zhang, Arun Bishop, Mac Schwager, and Zachary Manchester. Fast contact-implicit model predictive control. *IEEE Transactions on Robotics*, 40:1617–1629, 2024.
- [21] Gijeong Kim, Dongyun Kang, Joon-Ha Kim, and Hae-Won Park. Contact-implicit differential dynamic programming for model predictive control with relaxed complementarity constraints. In *2022 IEEE/RSJ International Conference on Intelligent Robots and Systems (IROS)*, pages 11978–11985. IEEE, 2022.
- [22] Gijeong Kim, Dongyun Kang, Joon-Ha Kim, Seungwoon Hong, and Hae-Won Park. Contact-implicit model predictive control: Controlling diverse quadruped motions without pre-planned contact modes or trajectories. *The International Journal of Robotics Research*, 44(3):486–510, 2025.
- [23] Bernhard Paus Graesdal, Shao Yuan Chew Chia, Tobia Marcucci, Savva Morozov, Alexandre Amice, Pablo Parrilo, and Russ Tedrake. Towards Tight Convex Relaxations for Contact-Rich Manipulation. In *Proceedings of Robotics: Science and Systems*, Delft, Netherlands, July 2024. doi: 10.15607/RSS.2024.XX.132.
- [24] Aykut Özgün Önel, Radu Corcodel, Philip Long, and Taşkın Padır. Tuning-free contact-implicit trajectory optimization. In *2020 IEEE International Conference on Robotics and Automation (ICRA)*, pages 1183–1189. IEEE, 2020.
- [25] Jonas Hall, Armin Nurkanović, Florian Messerer, and Moritz Diehl. LCQPow: a solver for linear complementarity quadratic programs. *Mathematical Programming Computation*, 17(1):81–109, 2025.
- [26] Alp Aydinoglu and Michael Posa. Real-time multi-contact model predictive control via admm. In *2022 International Conference on Robotics and Automation (ICRA)*, pages 3414–3421. IEEE, 2022.
- [27] Alp Aydinoglu, Adam Wei, Wei-Cheng Huang, and Michael Posa. Consensus complementarity control for multi-contact mpc. *IEEE Transactions on Robotics*, 2024.
- [28] Wei-Cheng Huang, Alp Aydinoglu, Wanxin Jin, and Michael Posa. Adaptive contact-implicit model predictive control with online residual learning. In *2024 IEEE International Conference on Robotics and Automation (ICRA)*, pages 5822–5828. IEEE, 2024.
- [29] Sharanya Venkatesh, Bibit Bianchini, Alp Aydinoglu, William Yang, and Michael Posa. Approximating global contact-implicit mpc via sampling and local complementarity. *IEEE Robotics and Automation Letters*, 2025.
- [30] Hien Bui, Yufei Yang Gao, Haoran Yang, Eric Cui, Siddhant Mody, Brian Acosta, Thomas Stephen Felix, Bibit Bianchini, and Michael Posa. Push anything: Single- and multi-object pushing from first sight with contact-implicit mpc. *arXiv preprint arXiv:2510.19974*, 2025.
- [31] Etienne Ménager, Pierre Fabre, Antoine Bambade, Wilson Jallet, Alberto de Marchi, and Justin Carpentier. Frictional Contact-Implicit Inverse Dynamics. working paper or preprint, August 2025. URL <https://hal.science/hal-05201780>.
- [32] Mihai Anitescu. Optimization-based simulation of non-smooth rigid multibody dynamics. *Mathematical Programming*, 105(1):113–143, 2006.
- [33] Marc Toussaint. A novel augmented lagrangian approach for inequalities and convergent any-time non-central up-

dates. *arXiv preprint arXiv:1412.4329*, 2014.

- [34] Joel AE Andersson, Joris Gillis, Greg Horn, James B Rawlings, and Moritz Diehl. Casadi: a software framework for nonlinear optimization and optimal control. *Mathematical Programming Computation*, 11(1):1–36, 2019.
- [35] Lorenz T Biegler and Victor M Zavala. Large-scale nonlinear programming using ipopt: An integrating framework for enterprise-wide dynamic optimization. *Computers & Chemical Engineering*, 33(3):575–582, 2009.
- [36] HJ Terry Suh, Tao Pang, Tong Zhao, and Russ Tedrake. Dexterous contact-rich manipulation via the contact trust region. *The International Journal of Robotics Research*, page 02783649251398875, 2025.

SUPPLEMENTARY MATERIAL

In the supplementary material, Appendices A and B clarify the theoretical stationarity interface used by IMPACT. Appendices C and D provide the hyperparameters used in our experiments and additional results.

Appendix A defines the corrected inner KKT residual r_{in} , whose multiplier set is consistent with the limiting normal cone of the complementarity set

$$\mathcal{C} := \{(Y, Z) : 0 \leq Y \perp Z \geq 0\}.$$

Appendix B proves that the BCD inner solver can attain this residual to any prescribed tolerance under the stated assumptions. This provides the inner-solve interface required by the safeguarded AuLa convergence result.

a) Scope: Throughout this work, “convergence/stationarity” refers to the standard safeguarded AuLa stationarity guarantee for MPCCs: under bounded safeguarded multipliers, vanishing inner residuals

$$r_{\text{in}}(w^k) \leq \epsilon_k, \quad \epsilon_k \downarrow 0,$$

and the stated MPCC regularity condition, every feasible accumulation point of the outer iterates is M-stationary¹ for the vertical MPCC formulation. We do not claim whole-sequence convergence, unconditional feasibility, or existence of accumulation points. By equivalence of the vertical reformulation, the stationarity statement also applies to the original MPCC after eliminating the slack variables.

APPENDIX A INNER STATIONARITY INTERFACE FOR THE SAFEGUARDED AU LA WRAPPER

This appendix makes explicit the inner-stationarity interface used by the safeguarded AuLa wrapper. The key point is that the complementarity variables are kept as hard constraints in the AuLa subproblem, and therefore the inner residual must be consistent with the limiting normal cone of the complementarity set

$$\mathcal{C} \doteq \{(Y, Z) : 0 \leq Y \perp Z \geq 0\}.$$

We use the M-stationarity convention of MPCC theory and of the safeguarded AuLa method of Guo and Deng [16]. In particular, the multipliers associated with the complementarity variables are not subject to a global sign restriction. Their admissible signs depend on the local complementarity status of each pair (Y_i, Z_i) .

Throughout Appendix A and Appendix B, we fix an outer iteration k and write

$$\Phi \equiv \Phi^k$$

for the corresponding inner AuLa objective in (4). The inner subproblem is

$$\min_{X, Y, Z} \Phi(X, Y, Z) \quad \text{s.t.} \quad (Y, Z) \in \mathcal{C}.$$

The smooth equality and inequality constraints of the original MPCC are already represented in Φ through the safeguarded AuLa terms. The complementarity set \mathcal{C} , however, is not penalized or relaxed.

a) Sign convention: We use the Lagrangian sign convention

$$\mathcal{L}_{\text{in}}(w, u, v) \doteq \Phi(w) - u^\top Y - v^\top Z, \quad w = (X, Y, Z).$$

Thus the complementarity normal-cone element is represented as

$$(-u, -v) \in N_{\mathcal{C}}(Y, Z),$$

where $N_{\mathcal{C}}$ denotes the limiting normal cone.

¹We refer the reader to [10] for the relevant notions of stationarity; these notions are classified by the signs and feasible sets of the multipliers associated with the complementarity constraints. Throughout this paper, we do not otherwise distinguish among them.

A. Stationarity-consistent multipliers and the KKT residual

For a feasible pair $(Y, Z) \in \mathcal{C}$, define the standard MPCC index sets

$$\begin{aligned} I_{+0}(w) &\doteq \{i : Y_i > 0, Z_i = 0\}, & I_{0+}(w) &\doteq \{i : Y_i = 0, Z_i > 0\}, \\ I_{00}(w) &\doteq \{i : Y_i = 0, Z_i = 0\}. \end{aligned}$$

We also define

$$\mathcal{Q}_M \doteq \mathbb{R}_{++}^2 \cup (\mathbb{R} \times \{0\}) \cup (\{0\} \times \mathbb{R}).$$

Equivalently, $(a, b) \in \mathcal{Q}_M$ if either $a > 0$ and $b > 0$, or $ab = 0$.

Definition 6 (Stationarity-consistent complementarity multipliers). For a feasible $w = (X, Y, Z)$ with $(Y, Z) \in \mathcal{C}$, define

$$\mathcal{M}_M(w) \doteq \left\{ (u, v) : \begin{aligned} u_i &= 0 \quad \forall i \in I_{+0}(w), \\ v_i &= 0 \quad \forall i \in I_{0+}(w), \\ (u_i, v_i) &\in \mathcal{Q}_M \quad \forall i \in I_{00}(w) \end{aligned} \right\}.$$

No sign restriction is imposed on v_i for $i \in I_{+0}(w)$, and no sign restriction is imposed on u_i for $i \in I_{0+}(w)$.

Lemma 7 (Normal cone of the complementarity set). For every feasible $(Y, Z) \in \mathcal{C}$,

$$N_{\mathcal{C}}(Y, Z) = \{(-u, -v) : (u, v) \in \mathcal{M}_M(w)\}.$$

Consequently, the condition

$$0 \in \nabla_{(Y, Z)} \Phi(w) + N_{\mathcal{C}}(Y, Z)$$

is equivalent to the existence of $(u, v) \in \mathcal{M}_M(w)$ such that

$$\nabla_Y \Phi(w) - u = 0, \quad \nabla_Z \Phi(w) - v = 0.$$

Proof: The complementarity set is a Cartesian product of the two-dimensional cones

$$C_i = \{(y_i, z_i) : 0 \leq y_i \perp z_i \leq 0\}.$$

For a single pair, the limiting normal cone is

$$N_{C_i}(y_i, z_i) = \begin{cases} \{0\} \times \mathbb{R}, & y_i > 0, z_i = 0, \\ \mathbb{R} \times \{0\}, & y_i = 0, z_i > 0, \\ \mathbb{R}_-^2 \cup (\mathbb{R} \times \{0\}) \cup (\{0\} \times \mathbb{R}), & y_i = 0, z_i = 0. \end{cases}$$

Writing each normal element as $(-u_i, -v_i)$ gives exactly the multiplier pattern in Definition 6. Taking the Cartesian product over all complementarity pairs gives the claim. \blacksquare

a) *Reference normal-cone stationarity measure:* The stationarity measure required by safeguarded AuLa/MPCC theory is

$$r_{\text{nc}}(w) \doteq \text{dist}_{\infty}(0, \nabla \Phi(w) + \{0\} \times N_{\mathcal{C}}(Y, Z)), \quad w = (X, Y, Z), \quad (Y, Z) \in \mathcal{C}. \quad (7)$$

Here dist_{∞} denotes distance in the ℓ_{∞} norm. This is the vertical-form version of the inner stationarity condition used in the safeguarded AuLa method of [16].

b) *X-block stationarity term:* In the theoretical formulation (4), the X -variables are unconstrained after the smooth constraints have been absorbed into the AuLa objective. Thus the X -block residual is

$$G^X(w) \doteq \nabla_X \Phi(w). \quad (8)$$

If an implementation additionally enforces simple convex bounds on X directly, then G^X may be replaced by the usual projected-gradient mapping over that convex set.

c) *Primal complementarity feasibility:* Although the inner subproblem enforces $(Y, Z) \in \mathcal{C}$ exactly, we keep the primal feasibility term in the residual to make the KKT certificate explicit:

$$r_{\text{pri}}(w) \doteq \max \left\{ \|\min(Y, 0)\|_{\infty}, \|\min(Z, 0)\|_{\infty}, \|Y \circ Z\|_{\infty} \right\}. \quad (9)$$

For all completed BCD iterates considered below, $r_{\text{pri}}(w) = 0$.

d) *KKT residual*: For any feasible $w = (X, Y, Z)$ and any $(u, v) \in \mathcal{M}_M(w)$, define

$$r_{\text{in}}(w; u, v) \doteq \max \left\{ \|G^X(w)\|_\infty, \|\nabla_Y \Phi(w) - u\|_\infty, \|\nabla_Z \Phi(w) - v\|_\infty, r_{\text{pri}}(w) \right\}. \quad (10)$$

The best achievable KKT residual is

$$r_{\text{in}}(w) \doteq \inf_{(u,v) \in \mathcal{M}_M(w)} r_{\text{in}}(w; u, v). \quad (11)$$

We call w ε -stationary for the inner AuLa subproblem if

$$r_{\text{in}}(w) \leq \varepsilon.$$

Equivalently, there exist consistent multipliers $(u, v) \in \mathcal{M}_M(w)$ such that $r_{\text{in}}(w; u, v) \leq \varepsilon$.

e) *Closed-form evaluation*: The infimum in (11) is separable across complementarity pairs. Let

$$a_i(w) \doteq \nabla_{Y_i} \Phi(w), \quad b_i(w) \doteq \nabla_{Z_i} \Phi(w),$$

and let $(s)_+ \doteq \max\{s, 0\}$. For feasible w , define the per-pair stationarity mismatch

$$d_i(w) \doteq \begin{cases} |a_i(w)|, & i \in I_{+0}(w), \\ |b_i(w)|, & i \in I_{0+}(w), \\ \min \left\{ \max \{ (-a_i(w))_+, (-b_i(w))_+ \}, |a_i(w)|, |b_i(w)| \right\}, & i \in I_{00}(w). \end{cases}$$

Then

$$r_{\text{in}}(w) = \max \left\{ \|G^X(w)\|_\infty, r_{\text{pri}}(w), \max_i d_i(w) \right\}. \quad (12)$$

At a biactive pair $(Y_i, Z_i) = (0, 0)$, the third case in d_i is precisely the ℓ_∞ -distance from (a_i, b_i) to the multiplier set \mathcal{Q}_M . This is the correction that replaces the incorrect global sign-feasible multiplier restriction.

B. Link to safeguarded AuLa stationarity

Lemma 8 (KKT residual matches the limiting-normal-cone residual). For every feasible $w = (X, Y, Z)$ with $(Y, Z) \in \mathcal{C}$,

$$r_{\text{nc}}(w) = r_{\text{in}}(w).$$

Proof: Since X is unconstrained in the inner AuLa subproblem (4),

$$\{0\} \times N_{\mathcal{C}}(Y, Z)$$

is the only nonsmooth normal-cone term in (7). By Lemma 7,

$$(-u, -v) \in N_{\mathcal{C}}(Y, Z) \iff (u, v) \in \mathcal{M}_M(w).$$

Therefore,

$$r_{\text{nc}}(w) = \inf_{(u,v) \in \mathcal{M}_M(w)} \max \left\{ \|\nabla_X \Phi(w)\|_\infty, \|\nabla_Y \Phi(w) - u\|_\infty, \|\nabla_Z \Phi(w) - v\|_\infty \right\}.$$

Using $G^X(w) = \nabla_X \Phi(w)$ and $r_{\text{pri}}(w) = 0$ for feasible w gives exactly $r_{\text{in}}(w)$. ■

Proposition 9 (Safeguarded AuLa interface). Suppose the inner iterates returned to the outer loop satisfy

$$r_{\text{in}}(w^k) \leq \varepsilon_k, \quad \varepsilon_k \downarrow 0.$$

Then the inner stationarity requirement of the safeguarded AuLa method,

$$\text{dist}(0, \nabla \Phi^k(w^k) + \{0\} \times N_{\mathcal{C}}(Y^k, Z^k)) \leq O(\varepsilon_k),$$

holds, up to norm-equivalence constants. Consequently, under bounded safeguarded multipliers and the MPCC regularity condition in [16, Thm. 3], every feasible accumulation point of the outer iterates is M-stationary for the vertical MPCC formulation.

Proof: The first claim follows immediately from Lemma 8 and norm equivalence between ℓ_∞ and Euclidean distance. The second claim is exactly the safeguarded AuLa convergence implication for MPCCs with the complementarity constraints kept as lower-level constraints; see [16, Thm. 3]. ■

a) *Takeaway*: The residual r_{in} is the sole inner-stationarity certificate used by the outer convergence statement. It is a computable KKT-style residual, but its multiplier feasibility is normal-cone consistent at the complementarity set.

APPENDIX B
 ε -STATIONARY ATTAINABILITY FOR THE BCD INNER SOLVER

This appendix proves that the BCD inner solver can attain the KKT residual r_{in} to any prescribed tolerance in finitely many inner iterations. This is the attainability property needed by the safeguarded AuLa outer loop. The result does not assert whole-sequence convergence of the nonconvex inner solver, nor does it assert global optimality of the AuLa subproblem.

Throughout this section, k is fixed and $\Phi \equiv \Phi^k$. We write

$$w^{(j)} = (X^{(j)}, Y^{(j)}, Z^{(j)})$$

for completed BCD iterates after the (Y, Z) -update. If the initialized value $(Y^{(0)}, Z^{(0)})$ is not the exact minimizer for $X^{(0)}$, all statements below apply after the first completed (Y, Z) -update, with a harmless relabeling of the index.

A. Assumptions

Assumption 1 (Smoothness and boundedness). Along the inner iterates $\{w^{(j)}\}$ generated at the fixed outer iteration k :

- 1) Φ is continuously differentiable on a neighborhood of the iterates, and $\nabla\Phi$ is Lipschitz on that neighborhood.
- 2) The sequence $\{w^{(j)}\}$ is bounded, and

$$\inf_{w: (Y, Z) \in \mathcal{C}} \Phi(w) > -\infty.$$

Assumption 2 (X -step sufficient decrease). There exists a constant $c_X > 0$ such that every completed BCD sweep satisfies

$$\Phi(w^{(j+1)}) \leq \Phi(w^{(j)}) - c_X \|G^X(w^{(j)})\|_\infty^2. \quad (13)$$

This assumption covers both one-step and multi-step X -updates. For example, it holds if the completed X -update is globalized by Armijo-type line search so that the accumulated decrease is comparable to the X -block residual, and the subsequent (Y, Z) -update does not increase Φ .

Assumption 3 (Exact (Y, Z) -block minimization over the complementarity set). For every completed BCD iterate $w^{(j)}$,

$$(Y^{(j)}, Z^{(j)}) \in \arg \min_{(Y, Z) \in \mathcal{C}} \Phi(X^{(j)}, Y, Z).$$

B. Descent and X -block attainability

Lemma 10 (Monotone decrease and square-summable X -block residual). Under Assumptions 1 and 2, the inner objective values are monotone non-increasing and

$$\sum_{j=0}^{\infty} \|G^X(w^{(j)})\|_\infty^2 < \infty.$$

Proof: Summing (13) from $j = 0$ to N gives

$$c_X \sum_{j=0}^N \|G^X(w^{(j)})\|_\infty^2 \leq \Phi(w^{(0)}) - \Phi(w^{(N+1)}).$$

By Assumption 1, the right-hand side is bounded above by

$$\Phi(w^{(0)}) - \inf_{w: (Y, Z) \in \mathcal{C}} \Phi(w).$$

Letting $N \rightarrow \infty$ proves square summability. Monotonicity follows directly from (13). ■

Theorem 11 (Attainability of the X -block residual). Under Assumptions 1 and 2, for any $\varepsilon > 0$, there exists a finite inner iteration index j_ε such that

$$\|G^X(w^{(j_\varepsilon)})\|_\infty \leq \varepsilon.$$

Moreover, for any $N \geq 0$,

$$\min_{0 \leq j \leq N} \|G^X(w^{(j)})\|_\infty \leq \sqrt{\frac{\Phi(w^{(0)}) - \inf_{w: (Y, Z) \in \mathcal{C}} \Phi(w)}{c_X(N+1)}}.$$

Proof: The quantitative bound follows from the summability estimate in Lemma 10. The finite-attainability statement follows because the right-hand side tends to zero as $N \rightarrow \infty$. ■

C. From X -block attainability to KKT inner stationarity

Lemma 12 (Exact (Y, Z) -minimization eliminates the (Y, Z) -part of the KKT residual). Under Assumptions 1 and 3, every completed BCD iterate $w^{(j)} = (X^{(j)}, Y^{(j)}, Z^{(j)})$ satisfies

$$r_{\text{in}}(w^{(j)}) = \|G^X(w^{(j)})\|_{\infty}. \quad (14)$$

Proof: By Assumption 3, $(Y^{(j)}, Z^{(j)})$ is a global, hence local, minimizer of the smooth function

$$(Y, Z) \mapsto \Phi(X^{(j)}, Y, Z)$$

over the closed set \mathcal{C} . The Fermat rule for closed sets gives

$$0 \in \nabla_{(Y,Z)}\Phi(w^{(j)}) + N_{\mathcal{C}}(Y^{(j)}, Z^{(j)}).$$

By Lemma 7, there exist multipliers

$$(u^{(j)}, v^{(j)}) \in \mathcal{M}_M(w^{(j)})$$

such that

$$\nabla_Y\Phi(w^{(j)}) - u^{(j)} = 0, \quad \nabla_Z\Phi(w^{(j)}) - v^{(j)} = 0.$$

The completed (Y, Z) -update is feasible for \mathcal{C} , so

$$r_{\text{pri}}(w^{(j)}) = 0.$$

Therefore the only nonzero term in the corrected residual (10) is the X -block term, and

$$r_{\text{in}}(w^{(j)}) \leq \|G^X(w^{(j)})\|_{\infty}.$$

The reverse inequality follows directly from the definition of r_{in} , since the X -block term appears inside the maximum in (10). Hence equality holds. \blacksquare

Theorem 13 (Attainability of MPCC inner ε -stationarity by the BCD inner solver). Fix outer iteration k and consider the completed BCD inner iterates $\{w^{(j)}\}$ generated by Algorithm 2. Suppose Assumptions 1–3 hold. Then, for any tolerance $\varepsilon > 0$, there exists a finite inner iteration index j_{ε} such that

$$r_{\text{in}}(w^{(j_{\varepsilon})}) \leq \varepsilon.$$

Moreover, for any $N \geq 0$,

$$\min_{0 \leq j \leq N} r_{\text{in}}(w^{(j)}) \leq \sqrt{\frac{\Phi(w^{(0)}) - \inf_{w: (Y,Z) \in \mathcal{C}} \Phi(w)}{c_X(N+1)}}.$$

Equivalently, there exist multipliers

$$(u^{(j_{\varepsilon})}, v^{(j_{\varepsilon})}) \in \mathcal{M}_M(w^{(j_{\varepsilon})})$$

such that

$$r_{\text{in}}(w^{(j_{\varepsilon})}; u^{(j_{\varepsilon})}, v^{(j_{\varepsilon})}) \leq \varepsilon.$$

Proof: Combine Theorem 11 with Lemma 12. The multiplier statement follows from the definition of r_{in} . \blacksquare

Practical stopping by stagnation. The implementation uses a budgeted inner solve and may stop by objective stagnation rather than explicitly evaluating r_{in} . The theory above is therefore an attainability statement. Nevertheless, the sufficient decrease condition gives the following useful calibration. If

$$\Delta_j \doteq \Phi(w^{(j)}) - \Phi(w^{(j+1)}) \leq \tau_k,$$

then (13) implies

$$\|G^X(w^{(j)})\|_{\infty} \leq \sqrt{\tau_k/c_X}.$$

By Lemma 12,

$$r_{\text{in}}(w^{(j)}) \leq \sqrt{\tau_k/c_X}.$$

Thus objective stagnation is a practical proxy for the KKT residual. The safeguarded AuLa convergence statement itself, however, uses the theoretical residual r_{in} and the attainability result in Theorem 13.

D. Empirical Results for the Stagnation-Based Stopping Rule

a) *Empirical validation of the stagnation-based stopping rule:* We empirically examine how the stagnation test relates to the corrected inner stationarity measure on the Push-T manipulation task. Across 30 random initializations (15,139 recorded inner-iteration pairs), we compute the association between

$$\|G^X(w^{(j)})\|_\infty$$

and the one-step objective-decrease proxy

$$\sqrt{\Delta\Phi(w^{(j)})}, \quad \Delta\Phi(w^{(j)}) \doteq \Phi(w^{(j)}) - \Phi(w^{(j+1)}).$$

By Lemma 12, for completed BCD iterates this quantity coincides with the KKT residual:

$$r_{\text{in}}(w^{(j)}) = \|G^X(w^{(j)})\|_\infty.$$

- **Strong correlation.** In log–log scale, the correlation coefficient is $\rho = 0.983$, indicating that the stagnation signal is a reliable empirical proxy for $\|G^X(w^{(j)})\|_\infty$ and hence for $r_{\text{in}}(w^{(j)})$.
- **Near-linear scaling.** A power-law fit yields an exponent of $0.945 \approx 1$, consistent with the theoretical $\mathcal{O}(\sqrt{\tau_k})$ dependence implied by the sufficient-decrease relation.
- **Empirical constant.** Empirically, we observe

$$\|G^X(w^{(j)})\|_\infty \leq c\sqrt{\Delta\Phi(w^{(j)})}$$

with $c \approx 1.9$ (equivalently, $c_X \approx 0.28$ in (13)).

Consequently, on Push-T, terminating the inner BCD loop when

$$\Phi(w^{(j)}) - \Phi(w^{(j+1)}) \leq \tau_k$$

typically yields

$$r_{\text{in}}(w^{(j)}) = \|G^X(w^{(j)})\|_\infty \leq 1.9\sqrt{\tau_k}. \quad (15)$$

We emphasize that (15) is an empirical calibration on this problem; the theoretical analysis only requires the existence of a sufficient-decrease constant.

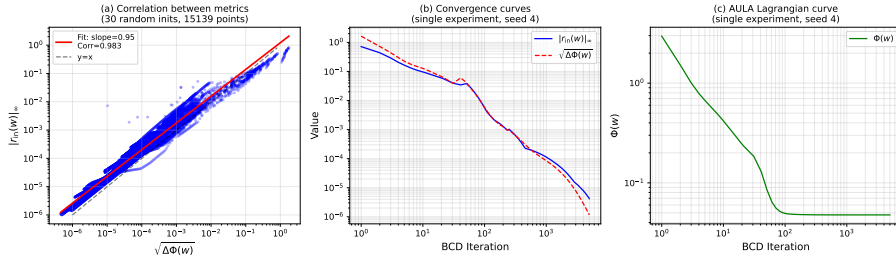


Fig. 5: Empirical validation of the stagnation-based stopping criterion on the Push-T task. (a) Log-log scatter plot showing the correlation ($\rho = 0.98$) between the X -block residual $\|G^X(w)\|_\infty$ (equivalently, the corrected inner residual $r_{\text{in}}(w)$ on completed BCD iterates) and the stagnation measure $\sqrt{\Delta\Phi(w)}$ across 30 random initializations (15,139 data points). (b) Convergence of both metrics during BCD iterations for a representative experiment. (c) Corresponding value of the augmented Lagrangian $\Phi(w)$.

APPENDIX C HYPERPARAMETERS AND EXPERIMENTS SETUP

A. CITO Benchmark Problems

Push Box Push Box is a planar pushing task where a rectangular box moves on a tabletop under friction. The solver must plan a long-horizon trajectory to reach target poses while selecting appropriate contact modes (which face is pushed) and corresponding contact forces, resulting in nontrivial mode switching.

Cart Transport Cart Transport involves indirect manipulation via friction: a payload rests on a cart and may stick or slip as the cart accelerates. The goal is to drive the system to a target while keeping the payload on the cart, often requiring non-monotone motions that exploit stick–slip transitions to reposition the payload.

Push T Push T generalizes planar pushing to a non-convex T-shaped object, increasing the number of feasible contact locations and modes. This leads to a larger complementarity system and a more complex mode landscape, making Push T a harder benchmark.

We follow the optimization problem formulation in CRISP [11] (in its Appendix B). Specifically, CRISP enforces the system dynamics as equality constraints, models unilateral contacts via complementarity constraints, and (for tasks such as Push-T) uses mutual-exclusion complementarity constraints to ensure that at most one control mode is active at each time step. For the Push-T and Cart-Transport tasks, we include the control-feasibility and boundary constraints within the MPCC formulation. In general, the objective terms and constraints are identical to those in CRISP.

We summarize the benchmark settings in Table II. The solver parameters are reported for IMPACT; for all other baselines, we set the stopping criteria to match this convergence setup.

TABLE II: Hyperparameters for the three benchmark tasks.

Parameter	Push Box	Push T	Cart Transporter
<i>Physical Parameters</i>			
Mass m (kg)	0.1	0.1	$m_1 = 0.1, m_2 = 0.2$
Gravity g (m/s ²)	9.81	9.8	9.81
Friction coefficient μ	0.5	0.4	0.2
Characteristic length (m)	$a = 0.3, b = 0.4$	$l = 0.05$	$l = 1.0$
Time step Δt (s)	0.05	0.05	0.02
<i>Problem Dimensions</i>			
State dimension n_x	3	3	4
Control dimension n_u	6	24	4
Complementarity pairs n_c	10	43	3
Equality constraints n_e	0	7	1
Inequality constraints n_i	0	4	4
<i>Optimization Parameters</i>			
Horizon	50	50	300
Stage control cost weight	0.001	0.01	10^{-6}
Final cost weight	100.0	100.0	5000.0
Multiplier Safeguard	10^6	10^6	10^6
ρ scaling factor	1.1	1.1	1.5
<i>Convergence Criteria</i>			
Max outer iterations	1000	1000	1000
Outer tolerance ϵ_h	10^{-5}	10^{-5}	10^{-5}
Outer tolerance ϵ_{comp}	10^{-5}	10^{-5}	10^{-5}
Max inner iterations	50	50	10
Inner tolerance	10^{-3}	10^{-3}	10^{-3}
<i>Newton Solver Parameters</i>			
Max Newton iterations	50	200	100
Newton tolerance	10^{-6}	10^{-6}	10^{-6}
Regularization	2×10^{-5}	5×10^{-5}	10^{-5}

B. Allegro Benchmark

We summarize the hyperparameters used in the Allegro benchmark tests in Table III.

APPENDIX D ADDITIONAL EXPERIMENT DEMONSTRATION

We provide additional experimental demonstrations here to build intuition for the main-text results.

A. IMPACT CITO Extra Demos

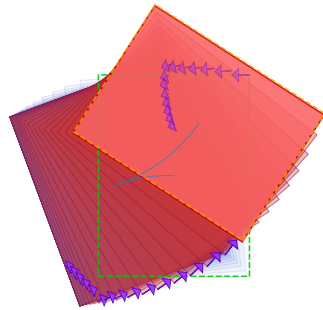
We include additional qualitative demos of IMPACT CITO on three tasks. Figures 6 and 7 report overlaid rollouts for the Pushing Box and PushT settings across multiple start–goal pairs in the (x, y, θ) state space. Figure 8 shows rollout sequences for the Cart Transporter task in (x, y, dx, dy) , with zero start and goal velocities. Visualization conventions (start/goal poses, force direction, and time progression) follow the figure captions. These results are based on the same data as the supplementary video.

TABLE III: Hyperparameters comparison for Allegro Hand in-hand manipulation: IMPACT vs. C-Free

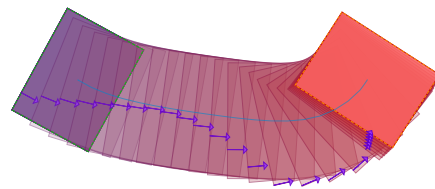
Parameter	IMPACT	C-Free	Notes
<i>System Dimensions</i>			
State dimension n_q	23	23	Same (obj: 7, robot: 16)
Velocity dimension n_v	22	22	Same (obj: 6, robot: 16)
Command dimension n_u	16	16	Same (joint position cmds)
Max contacts n_{con}	20	20	Same
<i>Simulation Parameters (Mujoco)</i>			
Time step h (s)	0.1	0.1	Same
Frame skip	50	50	Same
Friction coefficient μ	0.5	0.5	Same
<i>MPC Parameters</i>			
Horizon N	4	4	Same
Control bound	± 0.1	$\pm 0.1(0.2)$	
<i>Cost Function Weights (Path Cost)</i>			
Position cost weight	0.0	0.0	Same
Quaternion cost weight	0.0	0.0	Same
Contact cost weight	1.0	1.0	Encourage contact
Grasp closure weight	0.0	0.0	Same
Control cost weight	0.1	0.1	Same
Velocity penalty	0.1	–	Object Damping
<i>Cost Function Weights (Final Cost)</i>			
Final position weight	1000.0	1000.0	Same
Final quaternion weight	90.0	50.0	scale match
<i>Solver-Specific Parameters</i>			
IMPACT Parameters			
ρ_{max}	10^3	–	
ρ scale factor	5.0	–	
Max outer iterations	10	–	
Outer tol (ϵ_h)	10^{-3}	–	
Outer tol (ϵ_{comp})	10^{-3}	–	
Max inner iterations	5	–	
Newton max iterations	30	–	
Newton step tolerance	10^{-5}	–	
Newton obj tolerance	10^{-6}	–	
C-Free (IPOPT-based NLP)			
IPOPT max iterations	–	50	
Complementarity relaxation	–	> 0	Relaxed LCP
<i>Success Criteria</i>			
Position tolerance (m)	0.02	0.02	Same
Quaternion tolerance	0.04	0.04	Same
Consecutive success steps	20	20	Same
Max rollout steps	1000	1000	Same

B. Allegro Extra Demos

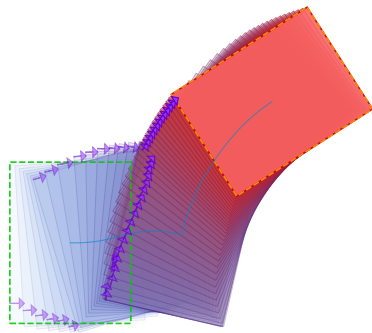
We provide additional Allegro in-hand re-orientation results on a variety of objects. Due to space constraints, we split them into four figures containing 5, 5, 5, and 2 objects, respectively (Figs. 9–12). The object shown above the hand indicates the target pose.



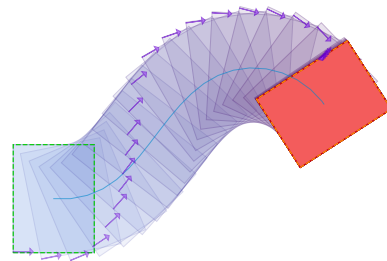
(a) From $(x, y, \theta) = (0.00, 0.00, 0.00)$ to $(0.10, 0.21, 1.00)$.



(b) From $(x, y, \theta) = (0.00, 0.00, -0.50)$ to $(2.00, 0.00, 1.00)$.

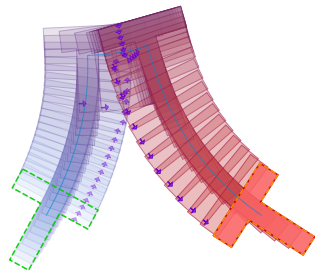


(c) From $(x, y, \theta) = (0.00, 0.00, 0.00)$ to $(1.00, 0.70, -1.00)$.

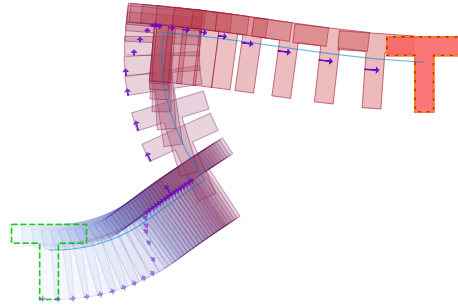


(d) From $(x, y, \theta) = (0.00, 0.00, 0.00)$ to $(2.00, 0.70, -1.00)$.

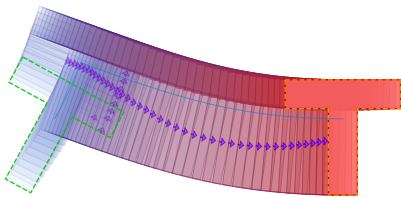
Fig. 6: Pushing Box task. Each panel overlays one rollout conditioned on a start and a goal state in (x, y, θ) . The green and orange dashed boxes indicate the start and goal poses, respectively. The purple arrow shows the pushing force, and the color gradient from light blue to orange indicates time progression. The blue solid line shows the trajectory of the box center.



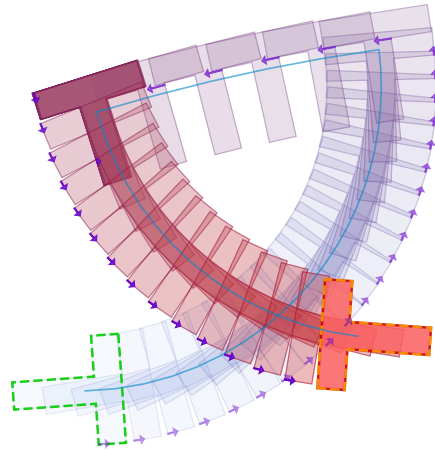
(a) From $(x, y, \theta) = (0.00, 0.00, -0.50)$ to $(0.50, 0.00, 1.00)$.



(b) From $(x, y, \theta) = (0.00, 0.00, 0.00)$ to $(1.00, 0.50, 0.00)$.



(c) From $(x, y, \theta) = (0.00, 0.00, -0.50)$ to $(0.50, 0.00, 0.00)$.



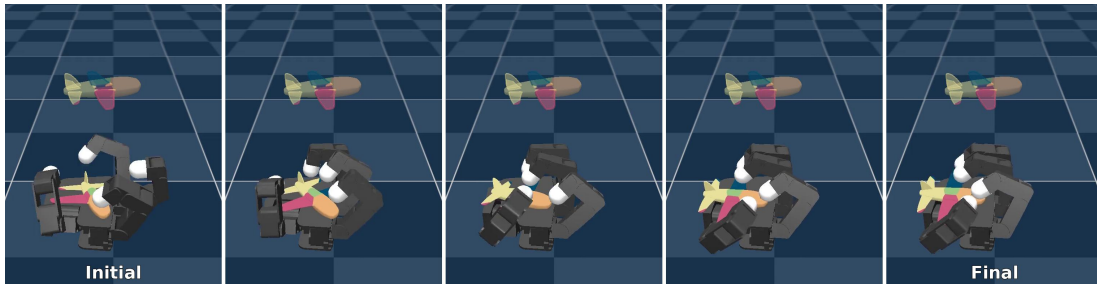
(d) From $(x, y, \theta) = (0.00, 0.00, -1.50)$ to $(0.50, 0.10, 1.50)$.

Fig. 7: Push T task. Each panel overlays one rollout conditioned on a start and a goal state in (x, y, θ) . The green and orange dashed boxes indicate the start and goal poses, respectively. The purple arrow shows the pushing force, and the color gradient from light blue to orange indicates time progression. The blue solid line shows the trajectory of the pushed object's center.

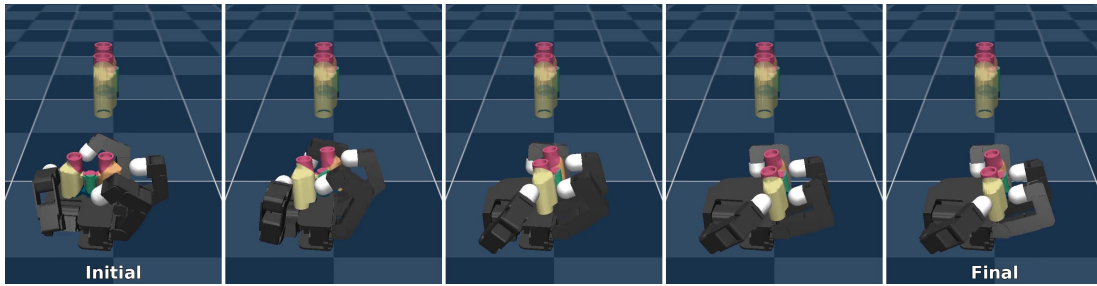


(a) Start at $x=0.00$, $y=0.00$. Goal is $x=0.00$, $y=0.90$.
 (b) Start at $x=0.00$, $y=-0.20$. Goal is $x=0.70$, $y=0.70$.
 (c) Start at $x=0.90$, $y=-0.10$. Goal is $x=1.70$, $y=1.50$.
 (d) Start at $x=1.00$, $y=1.00$. Goal is $x=-1.00$, $y=-1.50$.

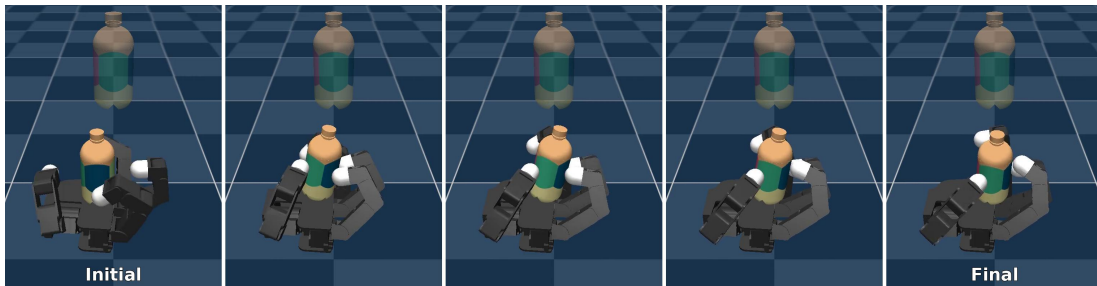
Fig. 8: Cart Transporter task. Each panel shows a rollout sequence in the state space (x, y, dx, dy) , where x and dx denote the load's position and velocity, and y and dy denote the cart's position and velocity, all expressed in the global coordinate frame. Start and goal velocities are set to zero.



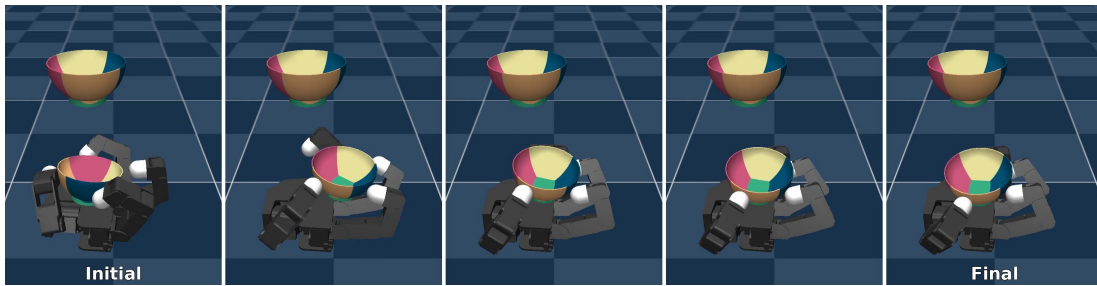
(a) Airplane



(b) Binoculars



(c) Bottle

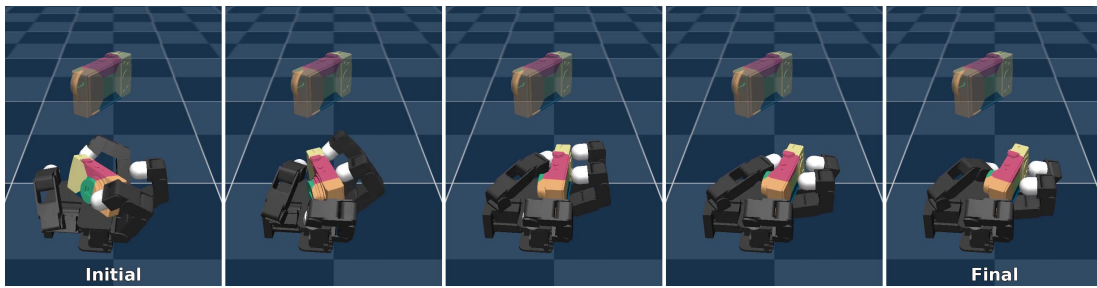


(d) Bowl

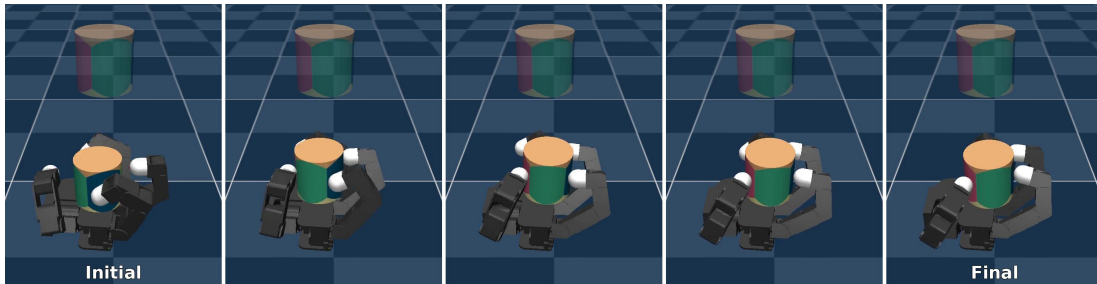


(e) Bunny

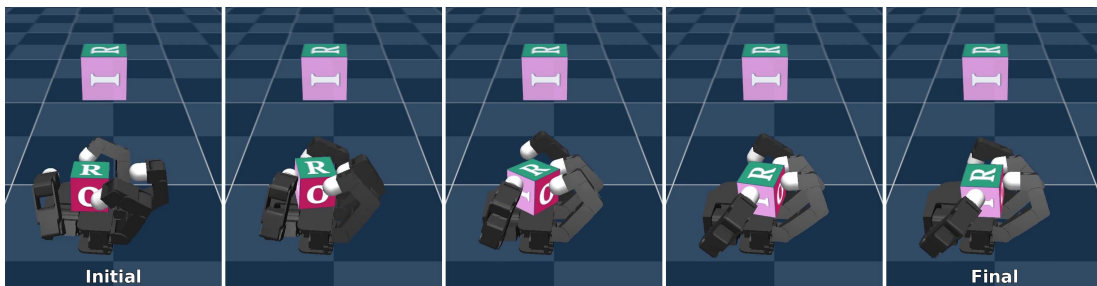
Fig. 9: Additional Allegro in-hand re-orientation results on: Airplane, Binoculars, Bottle, Bowl, and Bunny.



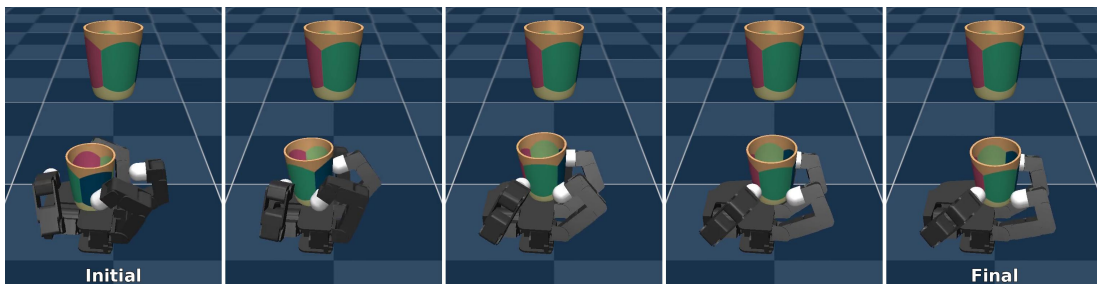
(a) Camera



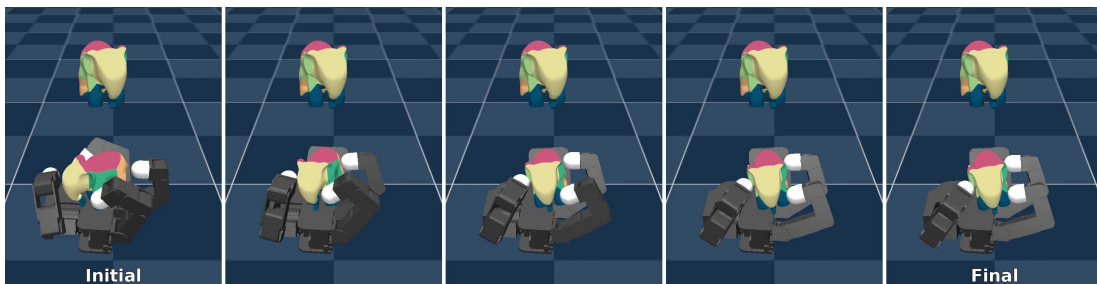
(b) Can



(c) Cube

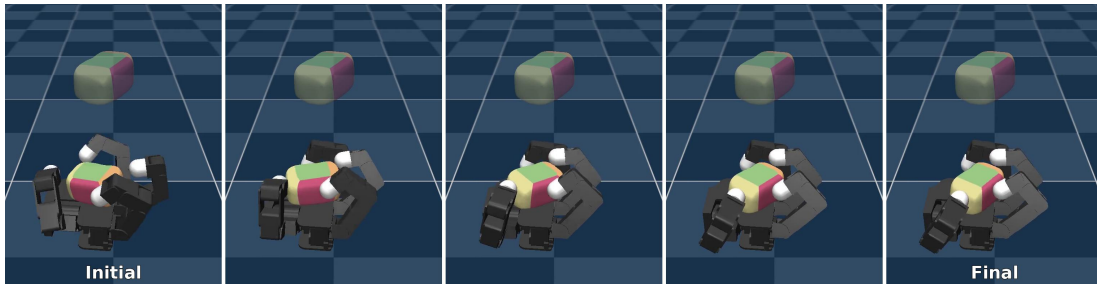


(d) Cup

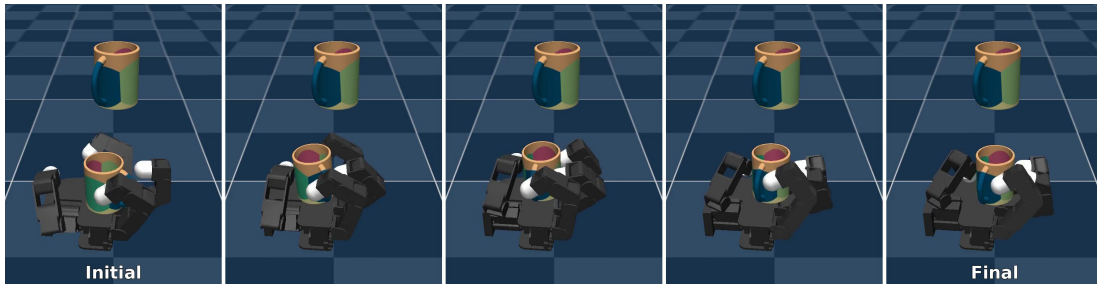


(e) Elephant

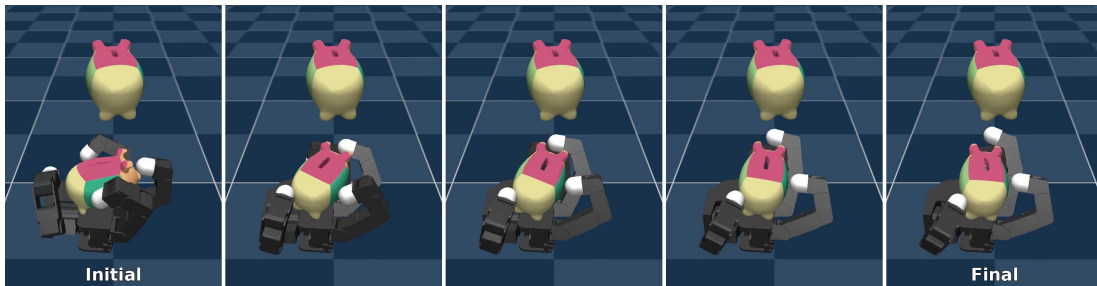
Fig. 10: Additional Allegro in-hand re-orientation results on: Camera, Can, Cube, Cup, and Elephant.



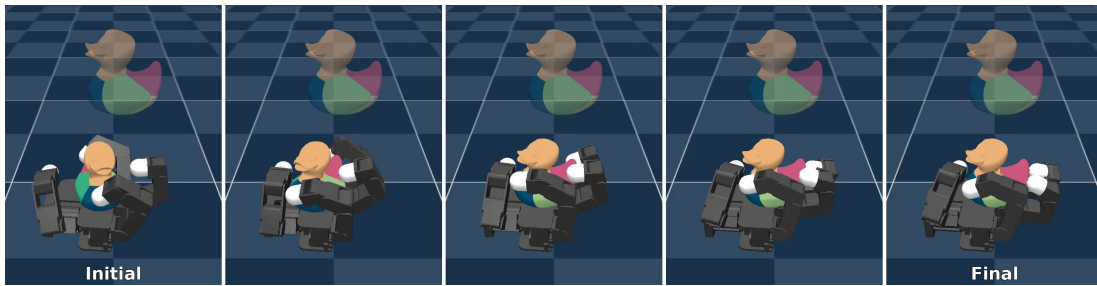
(a) Foam brick



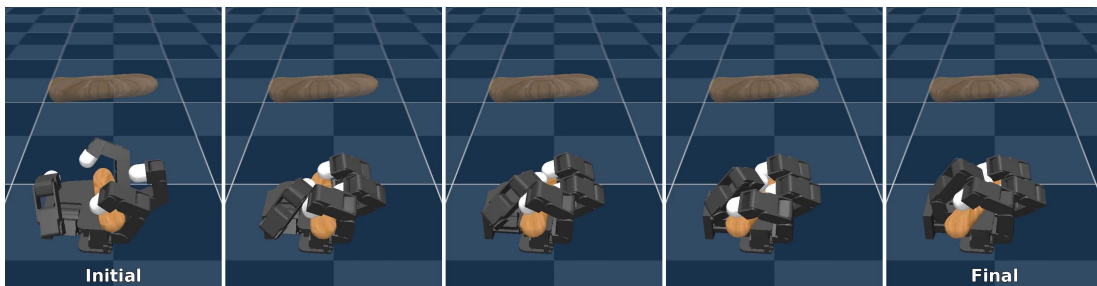
(b) Mug



(c) Piggy

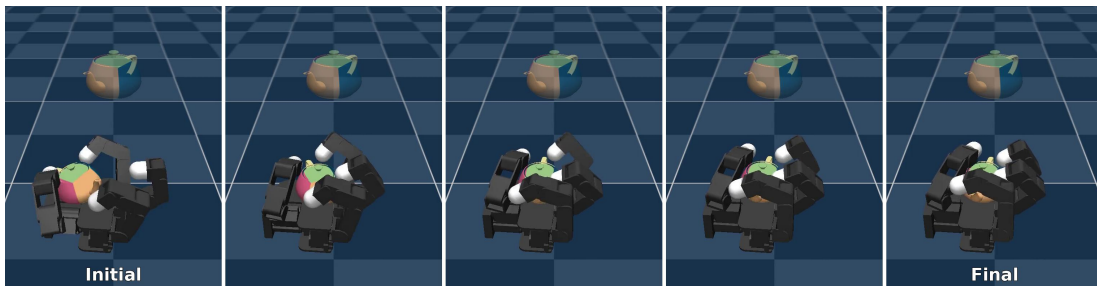


(d) Rubber object

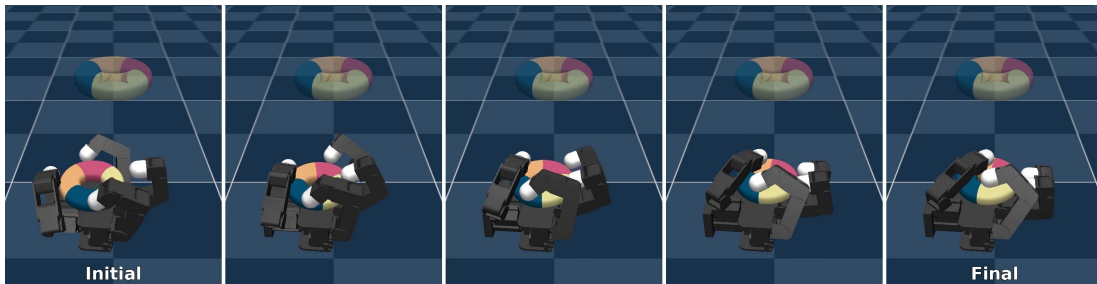


(e) Stick

Fig. 11: Additional Allegro in-hand re-orientation results on: Foam brick, Mug, Piggy, Rubber object, and Stick (fail example).



(a) Teapot



(b) Torus

Fig. 12: Additional Allegro in-hand re-orientation results on: Teapot and Torus.